Discrete Element Modeling of the Influence of Density and Confining Pressure on the Compression and Shear Behavior of Granular Materials

by

Andrew J. Walsh

B.S., Civil Engineering (1994)
University of Virginia

Submitted to the Department of Civil and Environmental Engineering in partial fulfillment of the requirements for the degree of

Master of Science in Civil and Environmental Engineering

at the

MASSACHUSETTS INSTITUTE OF TECHNOLOGY

May 1998

Author .....
Department of Civil and Environmental Engineering
May 26, 1998

Certified by .....
Charles C. Ladd, Professor
Department of Civil and Environmental Engineering
Thesis Supervisor

Certified by .....
John R. Williams, Associate Professor
Department of Civil and Environmental Engineering
Thesis Supervisor

Accepted by .....
Joseph M. Sussman
Chairman, Departmental Committee on Graduate Studies
Department of Civil and Environmental Engineering

Discrete Element Modeling of the Influence of Density and Confining Pressure on the Compression and Shear Behavior of Granular Materials

by

Andrew Walsh

Submitted to the Department of Civil and Environmental Engineering
on May 26, 1998, in partial fulfillment of the requirements for the
degree of Master of Science in Civil and Environmental Engineering.

Abstract

An understanding of the mechanical behavior of granular materials is complicated by the particulate nature of the media. The Discrete Element Method has proven to be an effective tool to model a granular mass by simulating the behavior of individual particles at the microscopic level in order to predict the behavior at the macroscopic level. One of the greatest limitations in using the method to date has been generating samples of a granular material at different densities. This thesis uses two methods to control the density of 800 elliptical shaped particles and then predicts stress-strain behavior during one-dimensional compression and drained shear in triaxial compression.

The first method to control sample density simulated Multiple Sieve Pluviation, a common preparation technique in experimental soil mechanics. Four parameters were varied to determine their effects on the final density of pluviated samples. Increasing the interparticle friction and increasing the width of the opening in the depositing hopper both consistently decreased the sample density. Varying the drop height and removing the diffuser sieves did not have consistent effects on the density. Although these trends are consistent with physical experiments, pluviation did not result in large changes in density. Hence particles were removed after deposition. With sufficiently high interparticle friction coefficients, this method generated stable samples having a greater range of densities.

After preparing samples at four different densities, one-dimensional compression tests were simulated. The simulations showed that samples with higher initial densities are stiffer as expected. However, density had little effect on the coefficient of earth pressure at rest. The final set of simulations modeled drained triaxial compression tests on samples at two different densities and three confining pressures. The higher density samples had higher peak stresses and exhibited greater dilation. Higher confining stresses decreased the friction angle and supressed dilation. The success of the simulations in duplicating the behavior found in physical experiments confirms the use of DEM for modeling granular materials.

Thesis Supervisor: Charles C. Ladd
Title: Professor, Department of Civil and Environmental Engineering

Thesis Supervisor: John R. Williams
Title: Associate Professor, Department of Civil and Environmental Engineering

Table of Contents

List of Figures

List of Tables

Chapter 1

Introduction

1.1 Discrete Element Analysis of Granular Materials

Over the past two decades, the Discrete Element Method has emerged as a useful tool for the computerized analysis of a wide variety of mechanics problems that involve discrete bodies. Discrete Element simulations analyze the forces and motion of physical systems and allow for motion of bodies independent of each other as well as contact forces between them. This makes the technique applicable to problems in soil mechanics, powder packing, and many other multi-body engineering problems.

Most research efforts to date on Discrete Element Methods have focused on developing efficient computer algorithms and expanding the capabilities of programs to model more complex behavior in physical systems. In its early years, practical applications of the method have been limited by the massive computation time required to model systems with a significant number of bodies. The subsequent development of faster computers and research to improve program efficiency has improved the practicality of using Discrete Element simulations, so that the field has been developed to the point that a wide range of tests can be performed. An important stage in the development of the Discrete Element Method is to apply it to different physical problems to determine its effectiveness as a realistic modeling tool.

Granular material analysis is one of the most natural applications of the Discrete Element Method. The macroscopic behavior of a granular material depends on the behavior of the constituent particles. Most physical testing procedures are not capable of measuring the motions and forces of individual grains, hence it is difficult to investigate the micromechanical behavior. The Discrete Element Method keeps track of each particle and allows

for measurements at both macroscopic and microscopic levels. This thesis attempts to simulate physical experiments performed on granular soils by using the Discrete Element Method to model the behavior of collections of particles.

1.2 Goals of Thesis

This thesis has three main goals relating to the use of Discrete Element Methods to analyze granular soils. The first is to show the viability of using the Discrete Element Method to simulate different types of physical experiments on granular soils. The second goal is to evaluate the ability of different methods to control the density of samples of granular soils. The final goal is to evaluate the effects of various experimental variables on the compression and shear behavior of the prepared samples.

The first type of experiment simulated is Multiple Sieve Pluviation. This is a procedure in which a granular soil is rained through sieves to prepare samples of different densities. This thesis creates a model of a Multiple Sieve Pluviation experiment and evaluates the effects of interparticle friction and geometrical parameters of the apparatus on the final density of a sample. A second experiment to vary the density of samples is by particle removal to simulate the inclusion of salt or sugar during sample preparation that will be subsequently dissolved by water. The joint goal of these simulations is to provide a reliable means of generating samples of varying densities.

The next group of simulations model one-dimensional (1-D) and triaxial compression tests on granular soils. In the 1-D tests, the initial density of the sample is varied to determine its effect on the stress-strain behavior and coefficient of earth pressure at rest (K_0). In the triaxial tests, both the initial density and the confining pressure are varied. The aim of these simulations is to determine the effects of the experimental variables on the simula-

tion results and to evaluate the ability of the Discrete Element Method to produce realistic results.

1.3 Outline of Thesis

This thesis has seven chapters. The second chapter reviews a number of topics that constitute the background for this work. Similar research and relevant published papers are also discussed. The third chapter describes the MIMES Discrete Element program that was used as the computational tool for the simulations performed. The experimental parameters used in the simulations for this thesis are included. Chapter Four presents the simulations to control the sample density using multiple sieve pluviation and the particle removal process. Chapter Five then describes simulations of 1-D compression tests of samples with varying initial densities. Chapter Six presents simulations of drained triaxial compression tests with varying initial densities and confining pressures. The final chapter summarizes the work performed, explains the significance of the results and how they fit into the development of Discrete Element Methods as a useful computer modeling tool, and recommends future areas of research in the field.

Chapter 2

Background

2.1 Overview of Particulate Mechanics

A granular material is a collection of interacting particles that are small relative to their surroundings. Each particle is relatively free to move as an independent body, but its behavior is governed by its mechanical contacts with its neighbors. The interaction of the particles with each other and their environment at the microscopic level controls the macroscopic behavior of the system as a whole. The field of particulate mechanics aims to understand the properties of the macroscopic material by investigating the behavior at the particulate level.

In the field of soil mechanics, the most common granular materials are sands and gravels which consist of particles of silicate minerals such as quartz and feldspar. Sands are classified as particles ranging in size from 0.06 mm to 2.0 mm in diameter and gravels range from 2.0 mm to about 15 mm in diameter (Lambe and Whitman 1969). A prime area of interest in particulate mechanics is the behavior of a collection of particles, such as sand, subjected to compression and shear. In a sample of sand, each grain exerts forces on the other grains it contacts. The force can be broken into a normal component and a tangential (shear) component from friction between the particles as shown in Figure 2.1. When an external force is applied to the system, the particles will move relative to each other until a state of equilibrium is reached. Interlocking of particles and interparticle friction provide the primary resistance to this motion. The strain of a sand under mechanical loading is a combination of the rearrangement of the geometrical configuration of the particles and the deformation and fracture of the individual grains. At low to medium strains

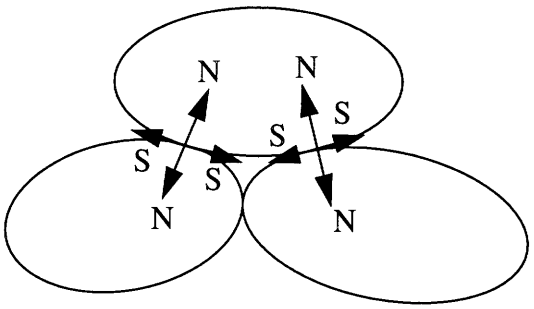

Figure 2.1: Resolution of Contact Forces into Normal (N) and Shear (S) Components

and stresses, the rearrangement dominates, as the particles slide and rotate relative to their neighbors and force chains between particles are formed and broken. This behavior leads to complex phenomena such as arching and the formation of circulation cells that further complicate the process (Williams and Rege 1997). At high stresses, particle deformation becomes the dominant mechanism and the material behaves more like a solid with less particle movement. If the forces on a particle are great enough, it will fracture and more rearrangement will take place. The separation of these two zones depends heavily on the initial density and configuration of the granular assembly and the strength of the particles.

As stated before, the goal of particulate mechanics is to determine how the motion and forces of individual particles govern the behavior of the overall granular medium. The large number of contacts makes it effectively impossible to derive constitutive laws for granular materials by working up from the particulate level (Lambe and Whitman 1969). However, while a micromechanical study may not generate exact values for macroscopic properties, trends at the particulate level can be examined to gauge their global effects. In contrast, physical experiments on a granular mass can not accurately measure the behavior of individual particles. While advanced methods such as high speed video, photoelasticity,

and piezosensitivity have been used to measure the behavior of individual particles in models of granular systems (Gourves 1992), any probe used to measure the behavior of a particle in a continuous particulate medium would affect the behavior of that particle and those around it (O'Connor 1996). Simple mechanical models exist for forces within small groups of particles (Christoffersen et al. 1981), but beyond a handful of particles the number of calculations required becomes impractical for a human to perform. The development of high-speed computers over the past few decades has led to the development of the *Discrete Element Method* (DEM), which is one of the most effective tools developed for simulating the behavior of granular materials at the particulate level.

2.2 Discrete Element Methods

The goal of the mathematical model of a physical process is to predict the behavior of an object or system to a reasonable level of accuracy (Bathe 1996). By averaging the properties of a material or environment on the microscopic level, it is often possible to model macroscopic behavior. A reliable model reduces the need for repeated physical testing that is often costly and subject to experimental error. Increased computing capabilities over the past few decades have made it possible to handle the large number of calculations required to model complex systems quite accurately.

The most widely used computer modeling technique in the field of mechanics is the Finite Element Method. Finite element modeling is an excellent tool for analyzing the structural mechanics of continuous materials. By evaluating a structure or process piecewise, the need to solve complex governing differential equations is avoided as numerical methods produce an approximate solution for the behavior of the body. Finite element methods are not suitable in some applications though, as they require that a system be rep-

resented as a continuum. This assumption is not appropriate for a number of physical processes where individual particles and local discontinuities affect the macroscopic behavior of an element being modeled as continuous. O'Connor (1996) states that the averages used in continuum models "do not pertain to the behaviour of the individual grain, the geometry of the grain, which grain rubs against some other grain, or which of them form intermediate structures that spontaneously appear and disappear." Dobry and Ng (1992) mention that attempts to use standard finite element techniques to model granular assemblies were made, but the process relied on reformulating the system stiffness matrix whenever a contact was made or broken. The number of calculations required proved impractical for assemblies with more than a few particles. This work, however, helped lead to the development of discrete element methods.

Discrete element methods (DEM) are computer simulation programs that model the interaction of independent bodies over time subject to physical laws of contact and motion. They were first developed in the early 1970s by Cundall and Strack for problems in geomechanics. Since then DEM has been used for a wide variety of applications including powder packing, sandstone disintegration during oil drilling, and fluid flow through a granular medium (Klosek 1997). There has also been research into incorporating finite element methods into DEM, but in most granular material applications the deformation of individual particles is sufficiently small that modeling particle deformations is not necessary to approximate the macroscopic behavior of the system (Cundall and Strack 1979).

The fundamental difference between DEM and finite element modeling of a granular material is that individual particles have their own velocity and force vectors in DEM simulations. Given an initial velocity or externally applied force, a particle will move a small

distance in a small time step. Each body can influence another body only through a force generated when the two come into contact. The sum of the contact forces on a body will give that body an acceleration that can be integrated over the time step to generate a new velocity and displacement. A fundamental assumption in the method is that if the timestep is small enough, any disturbance caused by the shifting of a particle will not propagate beyond its neighbors with which it is in contact. In general a smaller time step will improve the accuracy of the results. There is a critical timestep for any system above which the calculation errors propagate to make the model inaccurate, but any timestep below this value should correctly model the behavior for a given set of contact assumptions. The specifics of the DEM program used for this thesis are discussed in Chapter 3.

Discrete element models described in the literature differ in many important ways. The simpler methods experiment with planar disks while more advanced methods can deal with arbitrary shapes or three dimensional bodies. There are also differences in the size and type distribution of the particles used and the physical laws that govern particle interaction. There has also been a wide range of applications of discrete element methods in the literature. A number of simulations of experiments on granular soils are discussed later in this chapter.

Discrete element methods have been developed to the point where almost any aspect of micromechanical behavior can be included in a model. However, there are still capabilities that have not been fully developed. Rothenburg and Bathurst (1992) state that "a disappointing aspect of working with simulated assemblies of disks and spheres is related to the difficulty of controlling density of these systems". The two methods most often used for generating random assemblies of particles are compressing a "gas" consisting of fric-

tionless particles in order to achieve maximum density (Rothenburg and Bathurst 1992) and allowing particles to settle by gravity by a method such as pluvial deposition (Thornton 1992). Neither of these methods has been used to effectively control the density of simulated particle assemblies though. Ting et al. (1989) had success increasing the void ratio of a container of particles by shaking the container, but this method disturbs the initial fabric of the soil and does not control the change in density. Two methods that are used or proposed to vary the density of granular samples in soil testing may be useful, but have not yet been simulated. These are preparation of samples using multiple sieve pluviation and the inclusion of particles (e.g. salt or sugar) in the granular mass which can be removed by flowing water to dissolve these particles.

2.3 Geometrical Packing of Particles

The density of a granular material is directly related to the packing geometry of the particles. Both the packing density and the structural fabric of a material affect its mechanical properties. Lee and Dass (1993) state that "parameters describing the packing structures, such as particle shapes and sizes, their spatial distributions, locations of particle-particle contacts, and changes of these parameters under applied loads are required in order to model the constitutive behavior of granular materials using particulate mechanics theory". Discrete element models also require information of mass, contact stiffness, and frictional properties of both the particles and the container holding them.

The two main differences among models of granular materials are random versus ordered packing and the use of two dimensions versus three. The most realistic model uses three-dimensional random packing, but this type of model requires significantly more intensive calculations. Much can be learned from simpler representations, so most models

for particle packing problems are set up in two dimensions. In some cases it is unclear how well two-dimensional models represent real physical problems, but many of the geometrical constraints of three-dimensional problems can be observed using flat shapes on a plane.

In soil mechanics, the common values used to describe packing density are void ratio (e), porosity (n), and relative density (D_r). These are relationships between the total volume of a soil (V), the volume of voids (V_v), and the volume of solids (V_s) given by the following equations:

$$e = \frac{V_v}{V_s} \tag{2.1}$$

$$n = \frac{V_v}{V} \tag{2.2}$$

$$D_r = \frac{e_{max} - e}{e_{min} - e_{min}}(100 percent) \tag{2.3}$$

In equation 2.3, e_{max} is the void ratio of the soil in its loosest packing condition and e_{min} is the void ratio at the maximum packing. Thus, a soil in its loosest state has 0% relative density and in its densest state it has 100% relative density.

The parameter most often considered for two-dimensional models is the maximum packing fraction, which is the ratio of covered area to total area (Cumberland and Crawford 1987). The simplest model is to pack uniform, non-overlapping circles as closely as possible. The maximum packing fraction is achieved when the circles form a hexagonal lattice as shown in Figure 2.2a. The packing fraction of 0.9069 (n = 0.0931, e=0.103) is significantly denser than the value of 0.7854 (n = 0.2146, e=0.273) obtained by the concentric stacking of particles in a square lattice shown in Figure 2.2b. It is possible to achieve even lower values through the contribution of arching, but most stable packings of circles fall between these two values.

Figure 2.2: 2-D Sphere Packing Configurations - a) Hexagonal Lattice b) Square Lattice

The next level of complexity in a planar model is to fill the interstitial voids between the disks with smaller sized circles. By filling the voids in a hexagonal lattice with the largest possible sphere that will fit, the packing ratio of the system can be increased to 0.9503 (n = 0.0497, e=0.052). The other extreme is to fill the voids with very small particles also packed hexagonally. The maximum packing fraction achieved by this method is 0.9913 (n = 0.0087, e=0.0088) (Cumberland and Crawford 1987). By increasing the number of circle sizes, the packing density can always be increased, but the limit of 1 can never be reached using circles. It is possible to fully cover a two-dimensional plane using uniform hexagons, quadrilaterals, and triangles, but these have limited applications to granular material problems.

There has also been much theoretical research into the regular packing of three-dimensional spheres. By stacking square lattices to form a cubic stacking, the loose packing ratio is 0.5236 (n = 0.4764, e = 0.910). The densest regular packing ratio is with a rhombohedral stacking, which is basically layers of hexagonal lattices offset to pack more tightly. This configuration has a packing ratio of 0.7405 (n = 0.2595, e = 0.350). Unlike the cubic stacking, the rhombohedral stacking is in a state of equilibrium. For a solid body to be stable, it must be supported by at least three points (Cumberland and Crawford 1987). For

this reason, many looser packing configurations will collapse into a denser one with only slight disturbance.

Analysis of regular packings finds the maximum theoretical void ratios, but these maxima are rarely approached in real physical applications. Particles rarely line up in ordered positions and phenomena such as arching can further decrease the packing density in a sample. In a series of experiments with uniform steel balls, Scott (1960) found that the volume fraction of solids varied from 0.601 (n = 0.399, e_{max} = 0.664) to 0.637 (n = 0.363, e_{min} = 0.570). The upper value was termed "dense random packing" and was obtained by shaking a cylinder full of balls. The lower value was termed "loose random packing" and came from turning the container on its side and allowing the balls to settle back into place slowly. This shows that in general there is a reasonably small range of values for packing ratios of uniform spheres. However, most granular materials do not consist of uniform particles and there are different shapes, so a much greater range of densities is observed.

Granular soils can have a wide range of particle size distributions. Uniform sands are close to the mono-size sphere packing situation, but many soils have a large percentage of fines mixed in with sand grains and thus a much greater range of void ratios. According to Lambe and Whitman (1969) a clean, uniform sand has a maximum void ratio of 1.0 (n=0.50) and a minimum void ratio of 0.40 (n=0.29). A silty sand and gravel mixture can obtain a much denser packing though, as it has a maximum void ratio of 0.85 (n=0.46) and a very dense minimum void ratio of 0.14 (n=0.12). The maximum void ratio is increased when the range of particle sizes is small, the particle sizes are small, and the particles are more angular. When there is a greater range of particle sizes, the voids between the large particles can be filled by the smaller particles.

2.4 Multiple Sieve Pluviation for Granular Soils

One of the more difficult goals to achieve in soil mechanics experimentation is to ensure that a soil sample being tested is truly representative of the soil in its natural state in the ground. It is virtually impossible to take a sample directly from the ground without changing the stresses acting on the soil. With granular (cohesionless) soils, sampling also changes the density unless the soil has been solidified such as by freezing.

When it is not possible to obtain undisturbed samples or when one wants to test sands at different densities, it is necessary to prepare reconstituted samples. Sample preparation methods have significant effects on the deformation-strength properties of granular soils (Miura and Toki 1982), since a soil's fabric and stress and strain histories also affect its mechanical behavior. To simulate the state of the soil in the field, it is best to prepare a sample that has the same relative density, granular structure, and moisture content as the natural soil. Moisture content is reasonably simple to control, but it is important to uniformly distribute the water through the soil. Relative density and granular structure are more difficult to control during sample preparation.

There are various methods used to achieve differing types of packing in granular soils. Lo Presti et al. (1992) classify three groups as vibration (including tapping), tamping, and pluviation. Vibration consists of placing loose soil in a mold and then shaking or tapping the mold to cause densification. The current ASTM method (ASTM D4253) for determining maximum dry density of a soil uses an electromagnetic, vertically vibrating table and saturated soil. Tamping consists of again filling a mold with loose soil and subjecting the sample to hammer blows until a desired level of compaction is attained. These two methods both can achieve very high relative densities of soil, but their ability to replicate in situ

soil fabric is questionable. Some of the density achieved comes as a result of particle crushing which would not be representative of the ground state of the soil. Another drawback is that the vibration or impact process can lead to a segregation of different sized particles which results in non-uniform samples (Lo Presti et al. 1992).

Pluviation has become the method of choice for many experiments in the past decade or so. Pluviation is defined as "a rain of cohesionless soil particles in a mold. It is obtained by gravity and using appropriate diffusers" (Lo Presti et al. 1992). Pluviation simulates the formation of natural deposits formed by sedimentation (Rad and Tumay 1987) and therefore should create more realistic soil fabrics. Controlling the kinetic energy of the particles falling into the mold gives good control of the relative density. The pluviation method is preferable to the other methods because it produces negligible particle crushing, less segregation of particle sizes, more density control, and better repeatability. One drawback is that with soils having a high fines content, there is often segregation of different size particles outward from the center of the mold. This should not be a problem for most clean granular soils though.

Raining of particles has been used in experiments for decades, but the development of multiple sieve pluviation (MSP) by Miura and Toki (1982) has increased the use of the method. The technique consists of a hopper filled with granular soil above a series of diffuser sieves above a mold as shown in Figure 2.3. When the nozzle on the hopper is opened, the soil particles are spread as they pass through the sieves before entering the mold. The general principle for the process is that a higher energy of the particles entering the mold results in greater relative density. Although one cannot control the fabric of the soil, it is assumed that this vertical deposition is similar to the natural process.

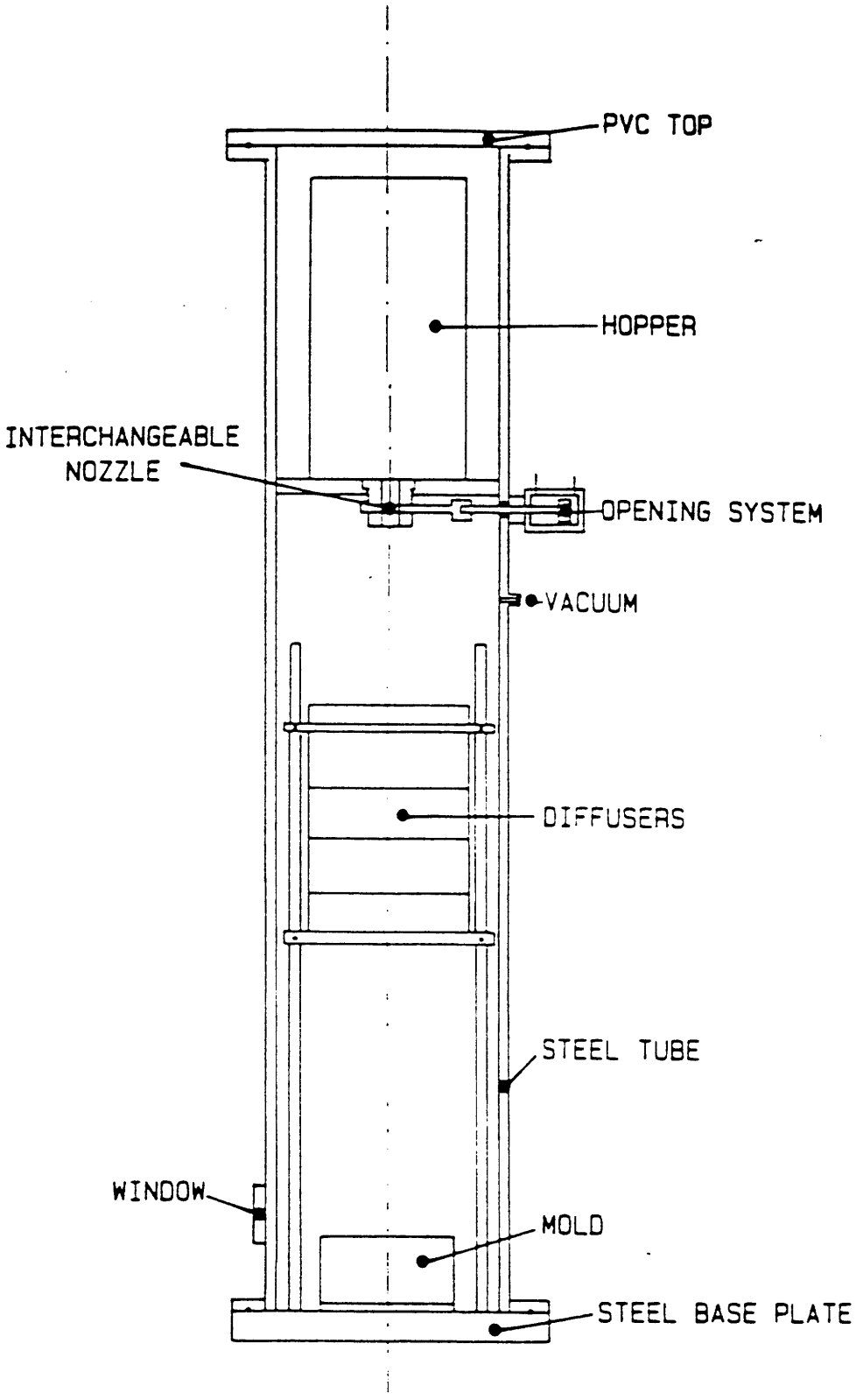

Figure 2.3: Multiple Sieve Pluviation Apparatus (from Lo Presti et al. 1992)

A number of factors affect the relative density of a soil achieved by MSP. Lo Presti et al. (1992) state that the three most important variables are the deposition intensity, the relative diffuser ratios, and the height of the drop from the hopper nozzle to the mold. The deposition intensity is the weight of soil falling per unit time. This is controlled by the diameter of the nozzle attached to the hopper. Interparticle interference due to the simultaneous fall of many particles results in loss of the kinetic energy of the particles. An increase in deposition intensity results in a decreased specimen density. This is considered the most important factor in the process. The relative diffuser ratios are the ratios of the sieve openings to the average and maximum diameters of the soil particles. Interparticle interference decreases as the relative diffuser ratios decrease. Consequently, relative density increases as the diffuser ratios decrease. A greater height of fall obviously increases the kinetic energy of the particles, but experimentation has shown that a critical height exists above which no further increases in relative density are achieved. Rad and Tumay (1987) state that factors such as the sand height in the hopper, distance between the diffuser sieves, and the number of sieves used in a diffuser have minimal effects on the relative density.

Lo Presti et al. (1992) performed an extensive series of MSP experiments on a number of different granular soils and varied a number of experimental parameters such as hopper nozzle opening size and drop height. Using a Messina Strait gravel (median particle diameter of 4.0 mm and a coefficient of uniformity of 3.5), increasing the hopper opening from 20 mm to 70 mm reduced the relative density of the sample from 100% to about 82% (approximate values from graph) for a drop height of 50 cm. Keeping the largest hopper nozzle opening, reducing the drop height to 20 cm reduced the relative density to 76%.

Increasing the drop height to 100 cm increased the relative density to 88%, but a further increase to a 180 cm drop height had no further increase, showing that there is a height above which drop height does not matter. A sample of Ticino sand was also tested. The sand had a median particle diameter of 0.54 mm and a coefficient of uniformity of 1.52. No data was reported for varying drop height, but increasing the width of the hopper opening from 5 mm to 70 mm caused a drop in relative density from about 105% to 40%. All of these experiments reflected the trends discussed above. While DEM simulations of MSP have not been reported in the literature, Thornton (1992) simulated the flow of particles through a hopper and the pluviation of particles into a bed as two separate experiments. These experiments were run using uniform 2-D circular particles. This work showed the feasibility of running these types of simulations, but no efforts were made to control the density of the pluviated samples.

Although multiple sieve pluviation provides a means of generating samples with a range of relative densities, Ladd (1997) suggested another method to attain very loose samples. By mixing sugar particles with a sand during sample pluviation, the sugar can be subsequently dissolved to produce additional voids in the sand skeleton. In theory, this enables preparation of samples with relative densities below 0%. Although this method has not been confirmed experimentally (to the author's knowledge), it seems to be a promising technique to produce low sample densities. It is uncertain as to how the large voids generated by the dissolution of the sugar particles affect the overall behavior of the sample, but much of the original structure in the sample should be preserved.

2.5 Drained One-Dimensional Compression Behavior of Granular Soils

There are a number of tests that are performed on granular materials to determine their stress-strain behavior. The simplest of these is a one-dimensional compression test, also known as an oedometer test. In this test, the sample is contained in a rigid ring that allows no horizontal expansion and is compressed by a rigid plate. Sometimes the top plate is driven at a constant velocity to create a constant strain rate. To limit the effect of the side wall friction, the mold can be treated with a friction reducing coating.

When the vertical force is applied, initial strain comes from rearrangement of particles and collapse of unstable particle contacts. Further strain requires greater stress as the contacts become more stable and there are less voids for particles to move into. This behavior is known as locking (Lambe and Whitman 1969). When the stress is great enough, particles begin to crush and there is temporary strain softening as the increased number of particles decreases the force per particle contact. This process continues cyclically as the smaller particles crush.

An important factor in the stress-strain behavior of an oedometer test is the initial density of the sample. With a loose sample, the greater volume of voids allows for more initial strain due to particle rearrangement. In a dense sample, the initial deformation is more heavily dependent on elastic deformation of the individual particles and the soil skeleton as a whole. This results in a much stiffer response as well as a smaller strain to cause particle crushing. As a loose sand compresses, its behavior becomes similar to a dense sand, but the soil fabric has changed significantly, so the results of a compressed loose sample will not be the same as an initially dense sample. While dense and loose sands exhibit the same general behavior, the degree varies significantly.

One useful parameter during 1-D compression is the ratio of the horizontal stress to the applied vertical stress. This ratio is known as the coefficient of earth pressure at rest (K_0). This ratio is related to the friction angle, ϕ, of a soil during virgin compression by:

$$K_0 = 1 - \sin\phi \tag{2.4}$$

This ratio assumes that there is no lateral strain in the ground, as would be the case if the deposit was formed by sedimentation. Sands formed like this have a K_0 value around 0.4 to 0.5 (Lambe and Whitman 1969). In a one-dimensional compression test, K_0 should remain approximately constant during virgin compression up to stresses that cause significant particle crushing.

There has been research into the discrete element simulation of one-dimensional compression tests. Bojtar and Bagi (1992) ran a series of DEM simulations of 1-D compression on assemblies of frictionless 2-D circles with varying sizes. Only thirty-two circles were used in each simulation, but even with this small sample the general trend of strain hardening with increasing load was observed. No variation of experimental parameters was reported. Ting et al. (1989) also simulated 1-D compression with two-dimensional circles, but more particles were used and the effects of different contact stiffnesses were considered. Higher interparticle contact stiffnesses resulted in higher values for the Young's modulus of the sample. It was observed that the circular particles rotated more than expected. Issa and Nelson (1992) ran DEM simulations of 1-D compression tests that allowed for the fracture of particles. As in other research, the simulations displayed strain hardening in tests with and without particle fracture. The increase in stiffness (hardening) came at a lower strain for the case without crushing as would be expected. All of these simulations showed that DEM can model the general behavior observed for granular soils, but as with most DEM simulations to date, most of the results that were reported focused

on qualitative trends as opposed to numerical results. None of the research tested the effect of varying the initial density of the samples.

2.6 Drained Triaxial Compression Behavior of Granular Soils

One drawback of the one-dimensional compression test is that it does not allow a soil to fail in shear. For this reason, another laboratory experiment that is often run is the triaxial compression shear test. A conventional triaxial compression test is performed by keeping the horizontal stress on a sample constant while driving a piston to compress the sample in the vertical direction at a constant strain rate. The horizontal stress is applied by placing a membrane around the sample and placing it in a pressurized cylinder. For a drained test, the fluid in the sample is allowed to enter or exit the sample during loading, so the volume of the sample does not remain constant. Diagrams of a triaxial testing cell are shown in Figure 2.4.

Much like the one-dimensional compression test, the major factor in the deformation of a soil during triaxial compression is the rearrangement of particles. Lambe and Whitman (1969) state that there are three stages in the straining process. The initial stage consists of a region of small strain with an almost linear increase in stress. During this region there is a slight decrease in volume. After this region the sample starts to yield and plastic (irrecoverable) strains occur. Dense soils dilate as the particles overcome interlocking by moving around each other. Failure is defined when reaching the peak stress. After the peak stress, soils experience strain softening. Part of this behavior is due to the formation of shear bands along which the deformation can occur more easily (Rege 1996). The final region consists of further straining under constant load and volume and is called the critical state or steady state.

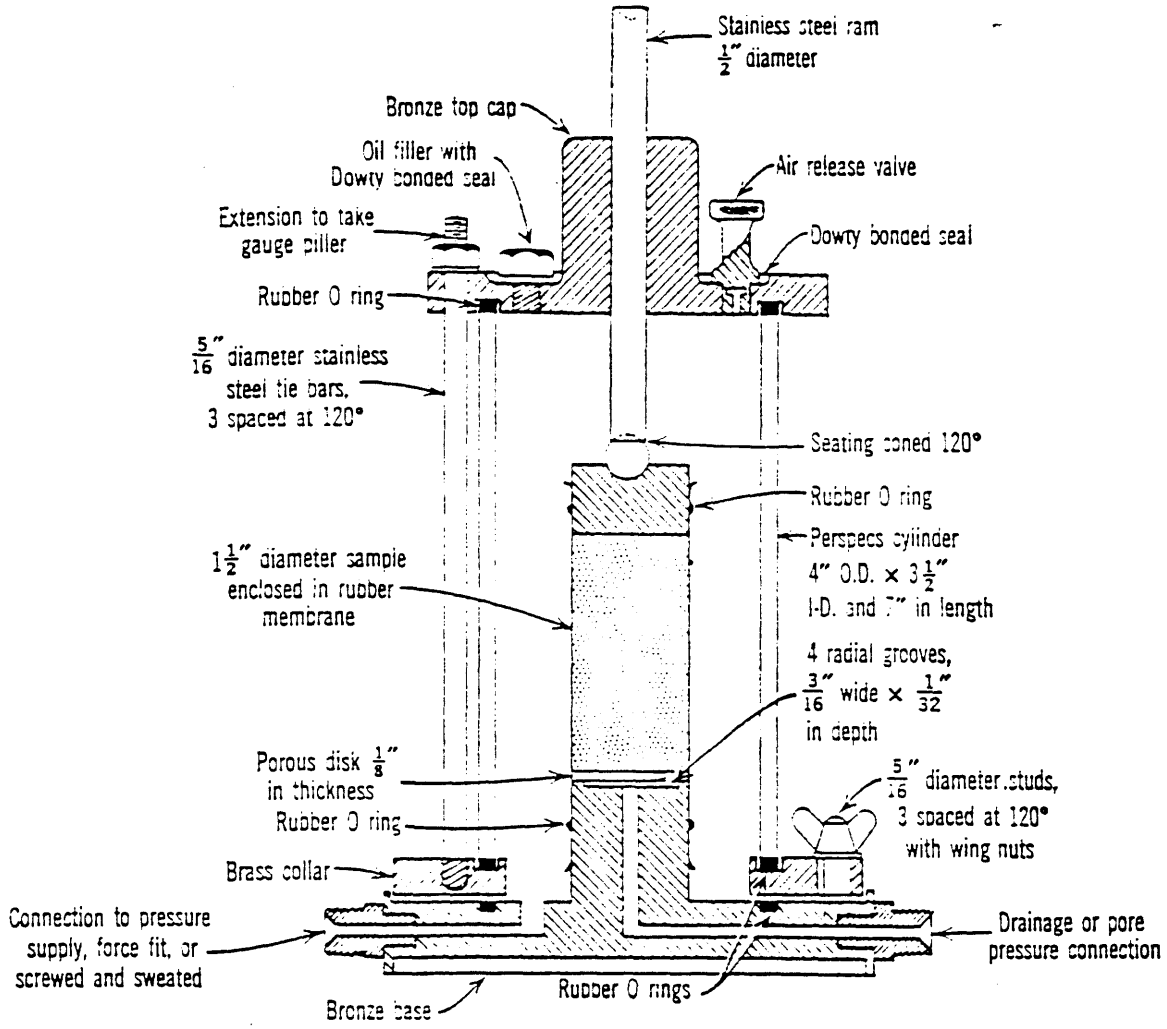

Fig. 9.5 Cross section of a typical triaxial cell. (From Bishop and Henkel, 1962.)

Figure 2.4: Drained Triaxial Compression Apparatus (from Lambe and Whitman, 1969)

Figure 2.5a plots the deviator stress (σ_1 - σ_3) versus axial strain for two specimens of sand under the same low confining stress with different initial void ratios. Figure 2.5b plots the volume change versus axial strain for the same samples. Figure 2.5 shows that initial density has a significant effect on the behavior of a sand during triaxial compression. A smaller initial void ratio increases the interlocking between the particles. This results in denser sands having a greater volume increase and an increased resistance at the peak strength due to the expansion (Lambe and Whitman 1969). Loose sands have much less volume increase and don't lose much strength after the peak stress.

Another major factor in a triaxial test is the level of confining stress. Figure 2.6 plots the stress-strain behavior of samples of sands with different confining stresses. As the confining stress increases, the peak normalized stress ($\sigma_1/\sigma_3 = (\sigma_1 - \sigma_3)/\sigma_c' + 1$) decreases. After the sample has yielded though, the confining stress has almost no effect on the normalized stress. Finally, the volume increase of the sample is lower for higher confining stresses. Most of these factors are a result of the confining stress increasing the frictional force between particles and decreasing interlocking by flattening particle contacts (Lambe and Whitman 1969).

There has been previous research using DEM to simulate drained triaxial compression tests. Ting et al (1989) simulated triaxial compression tests on assemblies of 2-D circles of different sizes. Experiments were performed with both rigid and flexible side walls. Other variables included confining stress, interparticle friction, and particle contact stiffness. Important trends that were observed were increased peak normalized stress and greater dilatancy with decreasing confining stress. Not much data was available for the effects of changing the sample density, but a reduction in void ratio did result in an increase in

a)

b)

c)

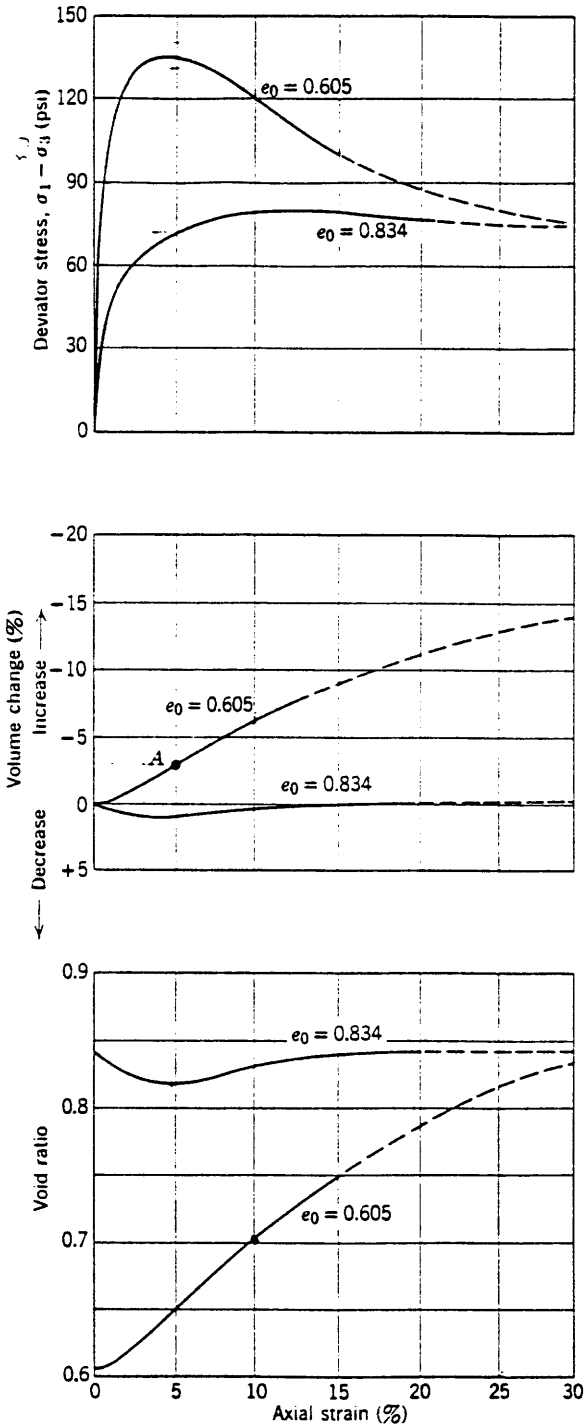

Fig. 10.18 Stress-strain curves for loose and dense specimens. Medium-fine sand. $\sigma_3 = 30$ lb/in.^{2}: $e_0 = 0.605 \approx 100\%\ D_r$; $e_0 = 0.834 \approx 20\%\ D_r$. Solid line, actual test data; dashed line, extrapolations based on results of other tests. (After Taylor, 1948.)

Figure 2.5: Drained Triaxial Test Behavior for Different Initial Densities (from Lambe and Whitman, 1969)

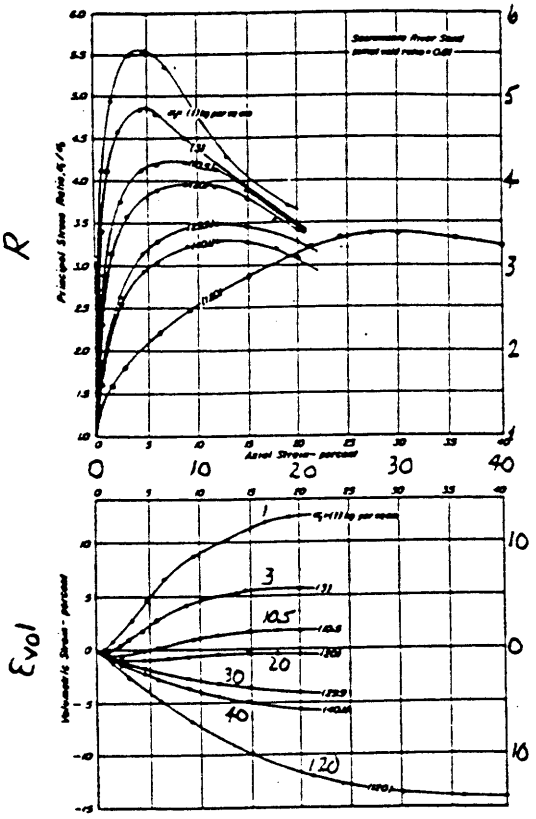

FIG. 3.—STRESS-STRAIN-VOLUME CHANGE DATA FOR DENSE SAND $D_r = 100\%$

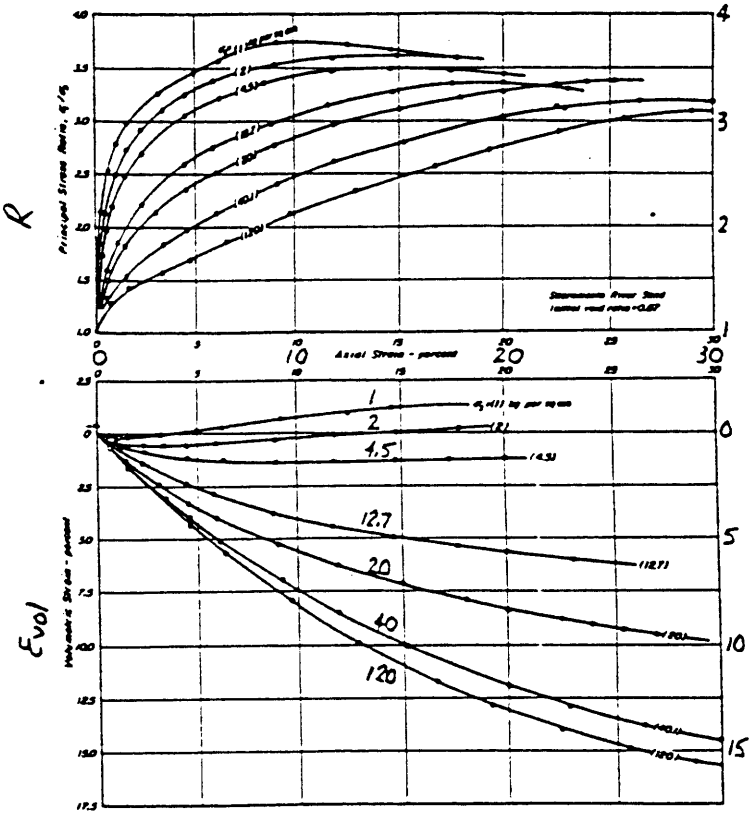

FIG. 4.—STRESS-STRAIN-VOLUME CHANGE DATA FOR LOOSE SAND $D_r = 38\%$

Figure 2.6: Drained Triaxial Test Behavior for Different Confining Pressures (from Lee and Seed 1967)

secant Young's modulus. As in the one-dimensional compression tests, excessive rotation of the circles was observed.

Rothenburg and Bathurst (1992) simulated triaxial compression with a variety of 2-D particle shapes ranging from circles to ellipses. These experiments showed that increased ellipse eccentricity resulted in a higher friction angle of a soil, but that there is a peak eccentricity after which the friction angle is reduced. Circular particles had the lowest friction angle. These experiments also varied the confining pressure and came out with the same expected results as Ting et al. mentioned above.

Rege (1996) performed 2-D simulations with multiple particles sizes to test the effects of particle shape and interparticle friction on the behavior of triaxial compression experiments. Samples of circles, ellipses, and diamonds were tested separately. The ellipses seemed to capture the true behavior of the triaxial test best, particularly with regards to dilation after the peak stress was reached. The most noticeable effect of increasing the interparticle friction was increased deviator stress at the same amount of vertical strain. Another set of tests modeled deformable side walls and found only slight changes from the rigid wall experiments. In analyzing individual particle behavior, it was also discovered that as a sample develops failure shear bands, groups of particles form circulation cells such that they rotate as a rigid body. This behavior would be very difficult to observe in physical experiments in which individual particle behavior can not be tracked.

Lin and Ng (1997) performed a fully three-dimensional simulations of triaxial compression using spheres and ellipsoids. Due to the computational intensity of a 3-D simulation, only small strain behavior was measured, but all expected stress-strain behavior was captured. Particle shape was the only experimental parameter varied. The ellipsoids had

greater deviator stress for the same level of vertical strain and a higher peak stress. It was also observed that ellipsoids underwent less rotation than the spheres in the simulation.

Chapter 3

The MIMES Discrete Element Analysis Program

3.1 Features and Capabilities

The MIMES discrete element analysis program was developed by Professor John R. Williams and former graduate student Nabha Rege at MIT's Intelligent Engineering Systems Laboratory. MIMES stands for Modeling Interacting Multibody Engineering Systems. The program is capable of modeling the dynamic behavior of systems of arbitrarily shaped two-dimensional bodies subjected to gravity and forces from contacts and collisions with each other. The program provides an animated display of the moving bodies and can also track the displacements and forces of each individual body over time. Rege (1996) states that all discrete element programs consist of four modules: system generation, contact detection, dynamics calculation, and visualization. This chapter describes each of the four modules in the MIMES program.

Any modeling environment must have parameters to accurately represent a real physical system. During system generation, MIMES allows the user to specify properties for the individual bodies and the environment in which they exist. This is done using a graphical user interface or commands and scripts with the Tcl/Tk language. For each body, a position, shape and material must be defined. MIMES simulations occur in a two-dimensional plane and the position of each object is defined in a standard 2-D coordinate system. It is possible to fix the velocity, rotation, and body forces of an object to constant values for the duration of a simulation. This is most useful to create stationary bodies by setting their velocities and rotations to zero. The plane extends infinitely in both directions, so any boundaries on a system must be created by generating bodies and fixing them in the plane. Two dimensional particles can be generated of any closed shape, but the most standard are

rectangles and superquadrics which includes circles, ellipses, and diamonds. Figure 3.1 shows a sampling of the different particle shapes that can be created. The size of the particles can be varied and any size and shape particles can interact with each other. Material parameters such as friction, density, and interparticle stiffness are also specified by the user. Each body in a simulation can have its own material parameters. Global parameters for the environment include acceleration due to gravity, a Rayleigh damping constant, and the timestep with which the simulation runs.

After generating the system, the simulation is run involving the contact detection and dynamics calculation modules. Contact detection takes up the majority of the computational effort and the time required increases with an increase in the number of particles. While MIMES implements efficient contact checking algorithms, it is necessary to limit the number of particles to have the simulations run in a reasonable amount of time. After the initial system is generated and contacts are identified, the simulation loop runs as described in the next section to determine the motions and forces of the particles.

Finally, the visualization module allows the user to see the particles in motion as the simulation runs and to track data for bodies in the system. Due to the limited speed of the program with a large number of particles, the visualization will occur much slower than real-time. To allow for more realistic visualization, MIMES allows the creation of movie files based on frames taken at a given interval. It is also possible to obtain a snapshot of the system at any given time. For each particle in the system, its position, velocity, and force can be tracked over time. The data for any individual body can be recorded for all timesteps and the data for all bodies can be recorded at any one timestep.

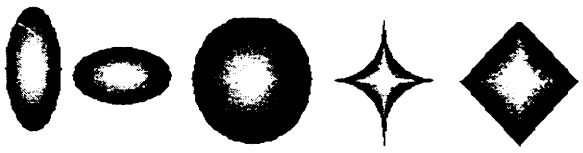

Figure 3.1: Different Shaped Particles in MIMES (from Rege 1996)

3.2 Simulation Loop

The MIMES simulation loop repeats the contact detection and dynamics calculation modules for the number of timesteps specified for the simulation. The first step in the loop is to initialize the gravitational and inertial body forces of the objects. Next, contacts between bodies are identified and the contact forces are calculated. Finally, the governing differential equation of motion is integrated and the loop is repeated. Summaries of the contact resolution and dynamics equation modules are presented here and are shown in greater detail in Rege (1996).

Contact resolution consists of first identifying which particles overlap with each other and are thus in contact at a given time and then determining the magnitude of the force generated at each contact. Since it would be very inefficient to check every pair of particles for possible contacts, MIMES implements an efficient spatial sorting algorithm, as described in O'Connor (1996), that partitions the simulation space into a grid and limits the checking of contacts to particles in the same vicinity. Most of the computation time is spent determining if two particles that are close to each other actually overlap, so this scheme improves the efficiency of the simulation greatly.

When two particles are identified as being in contact, they are added to a list that stores all current contacts. After the list of contacts is developed, the force between each pair of particles is calculated. MIMES uses "soft" contacts to determine the force between two particles. The particles are effectively rigid, but some deformation is assumed at the contact between particles. As shown in Figure 2.1, there are both normal and tangential components of forces at contacts between particles in a granular material. Figure 3.2 shows a schematic representation of how the contact is modeled. One spring with stiffness k_n models the normal contact and another with stiffness k_s models the shear contact. The friction between the two surfaces has an interparticle friction coefficient μ.

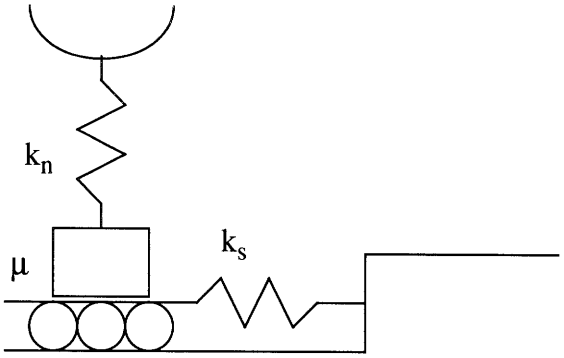

Figure 3.2: Schematic Representation of Contact (modified from Rege 1996)

The dynamics calculation module is based on Newton's second law that the sum of the forces on the body is equal to its mass times its accleration. Equation 3.1 shows the governing differential equation of motion, where $\underline{M}$ is the mass matrix for the particle, $\underline{K}$ is the stiffness matrix and $\underline{u}$ is the displacement vector in the normal and tangential directions and $\underline{F}$ is the body force vector:

$$\underline{M}\frac{d^2\underline{u}}{dt^2} + \underline{K}\underline{u} = \underline{F} \tag{3.1}$$

An explicit integration scheme is used to solve this equation and is described in detail by Rege (1996).

When the simulation runs, one of the biggest concerns is selection of an appropriate timestep. Due to the nature of the soft particle contacts, a timestep that is too large will result in the system becoming unstable. Particle overlaps will be too great, so the resulting forces will overcompensate and two particles will "explode" away from each other by flying off in opposite directions at great velocities. Also related to the timestep problem is the need to control the damping in the system. In solving the differential equation, Rayleigh damping is accounted for by effectively having all motion occur in a viscous medium, thus reducing the kinetic energy of all of the particles. If a system is significantly underdamped, it is possible for a bed of particles to vibrate without stopping, leading to addi-

tional settlement or further instabilities in the system. If a system is overdamped though, it is possible to prevent particles from attaining their true equilibrium positions over the duration of a simulation. Both of these concerns depend on the geometric and material parameters of the bodies in the simulation.

3.3 Selection of Simulation Parameters

The selection of the bodies and their parameters attempted to capture the most important aspects of granular soil behavior. Uniform ellipses were used for the particles in all of the simulations. Real sand particles are close in shape to ellipses (Lin and Ng 1997). Previous DEM research has found that circular particles roll too much during experiments that model granular materials (Ting et al. 1989). Research has been done using multiple sizes of sand grains in the same simulation, but it was decided that it would be better to understand the behavior of uniform particles before testing a mixture of sizes. The principal axes of the grains were set to 3 mm and 4mm based on Messina Strait Gravel used in MSP experiments by Lo Presti et al. (1992). This size was chosen to allow for realistic testing apparatus dimensions without needing too many particles. 800 particles were used for each simulation. In previous experiments, Rege (1996) found that there was little difference in results using 800 and 2000 particles and concluded that 800 was a large enough sample to capture the system behavior.

The density of the particles was specified as a mass per unit area. Sand grains are three-dimensional bodies, but MIMES only represents them as two-dimensional planar shapes. The particles act as if they are long rods that only undergo plane strain. The specific gravity of most sand particles is about 2.5, so the density is 2500 kg/m^3. The two-dimensional density used in these simulations was 1000 kg/m^2. This value was selected based on values used in previous research with MIMES. Although this value is somewhat arbitrary, the main significance is the relation between the density times accleration due to

gravity and the contact stiffness of the particles. The acceleration due to gravity was selected as the standard 9.81 m/s^2. The interparticle contact stiffness was then selected based on the weight of the particles under gravity. The selection of these parameters affects the magnitude of the forces measured, but the shape of any force deformation curves should be the same.

The spring stiffness in soft contact models is usually chosen based on Hertzian contact theory (Rege 1996). However, the main concern is to minimize the overlap of the particles for the given physical process being simulated. Based on previous experiments and visual observation of experiments using the chosen particle density, an interparticle contact stiffness of 1.0×10^6 N/mm was selected. Visual observation indicated that this value approximated rigid contacts with little particle overlap under moderate stresses. A more realistic model would have had a different contact stiffness between the particles and the mold holding them, but the value is again dependent on the weight of the particles. For this work, the same stiffness was used. The coefficient of friction between the particles was varied in the simulations. Values of 0.1 and 0.5 were chosen based on previous MIMES experiments.

The timestep and damping used were both selected based on the other simulation parameters, as well as the physical process being simulated. If the timestep is too large, the particle overlaps become too large to model the contact forces accurately. This results in particles exhibiting physically impossible behavior, such as passing through other bodies at very high velocities. For the Multiple Sieve Pluviation simulations described in Chapter Four, a time step of 5×10^{-5} seconds was chosen to obtain reasonable particle behavior. The same timestep was chosen for the one-dimensional and triaxial compression tests described in Chapter Five and Chapter Six. This kept the particles stable throughout the range of applied stresses of interest.

Since the damping acts on all particles as a viscous medium, the value was chosen low enough to allow particles to move through space realistically, but high enough to prevent a settled bed of particles from vibrating uncontrollably. For the Multiple Sieve Pluviation experiments, the greatest concern was to allow the particles to fall under gravity as if there was minimal resistance from the atmosphere. Based on previous MIMES experiments, a very low value of 2.5 was chosen for the Rayleigh damping constant. After deposition, the bed of particles was able to come to equilibrium with this damping. For the one-dimensional and triaxial compression experiments, the greater concern was the oscillation of the particles when subjected to stress. By measuring the time required for a stress wave to travel through the bed of particles, a damping constant of 300 was chosen. Graphs with results from these simulations came out much smoother with this value than with lower values.

Chapter 4

Multiple Sieve Pluviation Simulations

4.1 Experimental Program

The first series of simulations tested the use of Multiple Sieve Pluviation (MSP) to control the density of granular assemblies. Particles were rained from a hopper through diffusing sieves into a receiving mold. The density of the granular assembly was measured after the particles had settled and experimental parameters were varied to evaluate their effects on the process.

As described in Chapter 3, 800 elliptical particles with principal axes of 3 mm and 4 mm were used for the granular media. The particles were all of the same material with a density of 0.001 kg/mm^2 and a contact stiffness of 1.0 x 10^6 N/mm as discussed in Section 3.3. The experimental "apparatus" consisted of a fixed hopper, a fixed receiving mold, fixed cross sections of sieve wires, and elliptical particles. As shown in Figure 4.1, the hopper was constructed with two vertical rectangular sidewalls and a funnel created from two rectangles rotated forty-five degrees inward from the bottom of the sidewalls. The mold consisted of two vertical rectangles attached to a bottom horizontal rectangle. In all experiments the mold was 100 mm wide. In some of the experiments, sieves were included by adding circular wires placed 160 mm and 180 mm above the bottom of the mold. Two layers of wires were created and staggered so that the bottom layer wires were below the middle of the spaces between the upper layer wires. This models the forty-five degree rotation of consecutive sieves in Miura and Toki's physical apparatus. The wires were 2 mm in diameter and spaced 10 mm center to center. The contact stiffness between the container walls and the particles was 1.0 x 10^6 N/mm and the walls were frictionless.

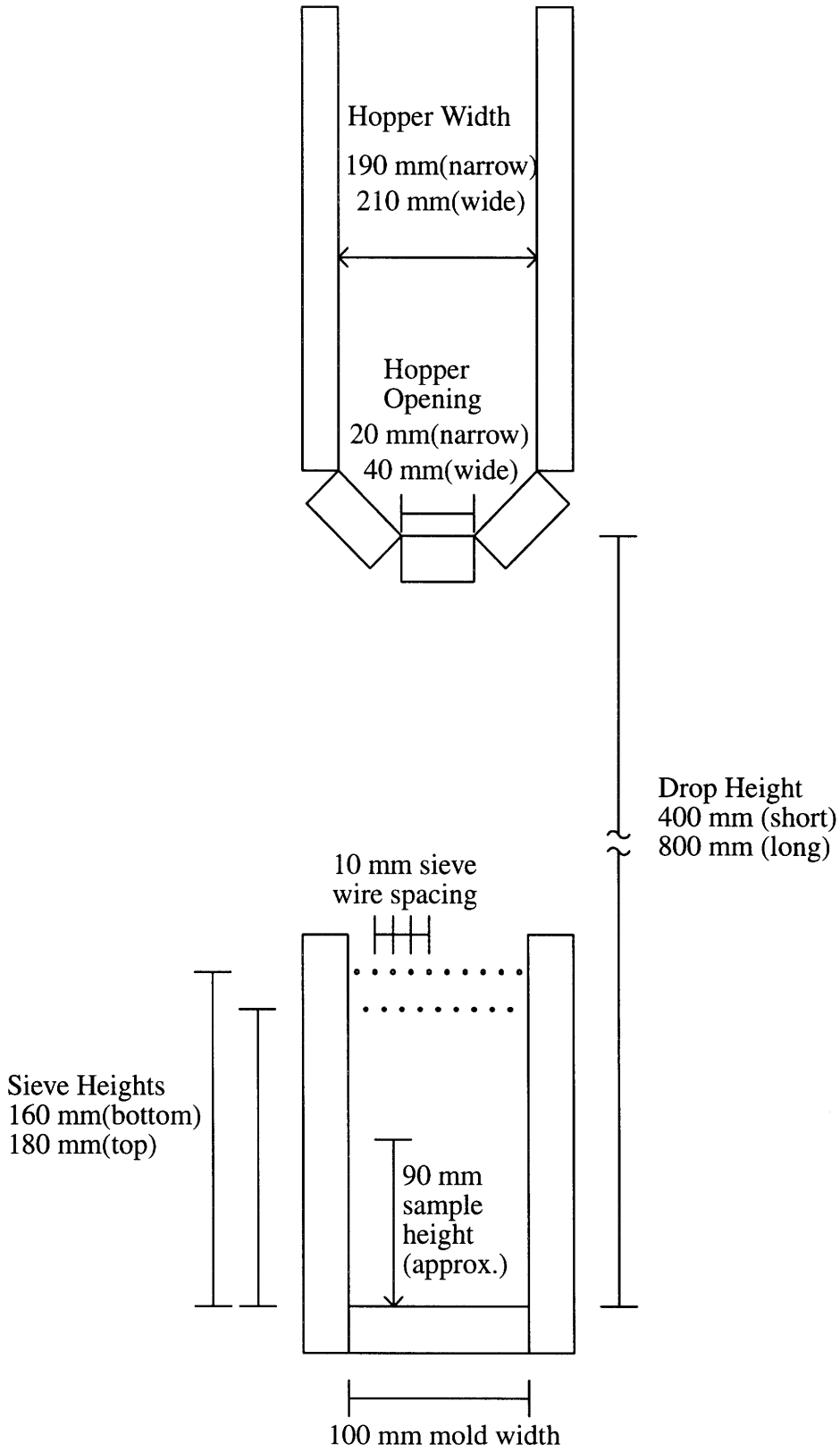

Figure 4.1: MSP Simulation Apparatus

The other constant simulation parameters were a Rayleigh damping coefficient of 2.5 and a timestep of 5×10^{-5} seconds.

A number of experimental parameters were varied to determine their effects on the final density. The two sizes for the opening of the hopper were 20 mm and 40 mm. The width of the hopper also varied with that change, as the hopper with the 20 mm opening had a total width of 90 mm and the hopper with the 40 mm opening had a total width of 110 mm. The height of the drop of the particles from the hopper opening to the bottom of the receiving mold had values of 400 mm and 800 mm. The interparticle coefficient of friction had values of 0.1 and 0.5. Finally, the sieves were removed in some experiments. Sixteen separate simulations were run to allow for all combinations of the variables.

4.2 Behavior of Simulations

The particles were generated in space above the hopper in rows with each particle having a random initial rotation. A plug was placed in the bottom of the hopper and the rows of particles were allowed to settle under gravity into the hopper. After removing the plug from the hopper, the particles began to fall from the hopper to the receiving mold below. Figures 4.2 and 4.3 show series of still frames from two MIMES simulations of the MSP process. Figure 4.2 show a simulation with a 40 mm wide opening on the hopper and Figure 4.3 shows a simulation with a 20 mm wide hopper opening.

Certain behavioral patterns were apparent from watching the simulations in progress. With the wide hopper opening, the particles flowed out in mass resulting in a shorter time to complete the simulation. As evident from Figure 4.2, the intensity of deposition was very high, resulting in significant interparticle interference even after the particles left the hopper and a dense concentration of particles around the sieves. Figure 4.3 shows that the smaller hopper opening results in individual particles falling almost independent of each other with much less interference until the sieves are reached.

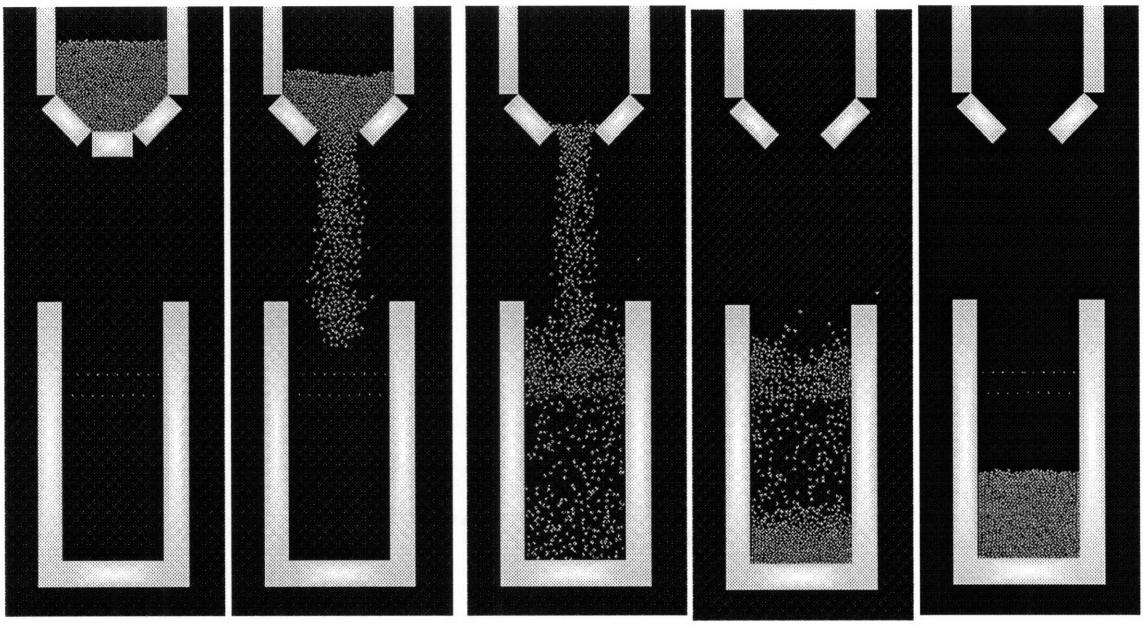

Figure 4.2: MSP Simulation (J) with Wide Hopper Opening (40 mm)

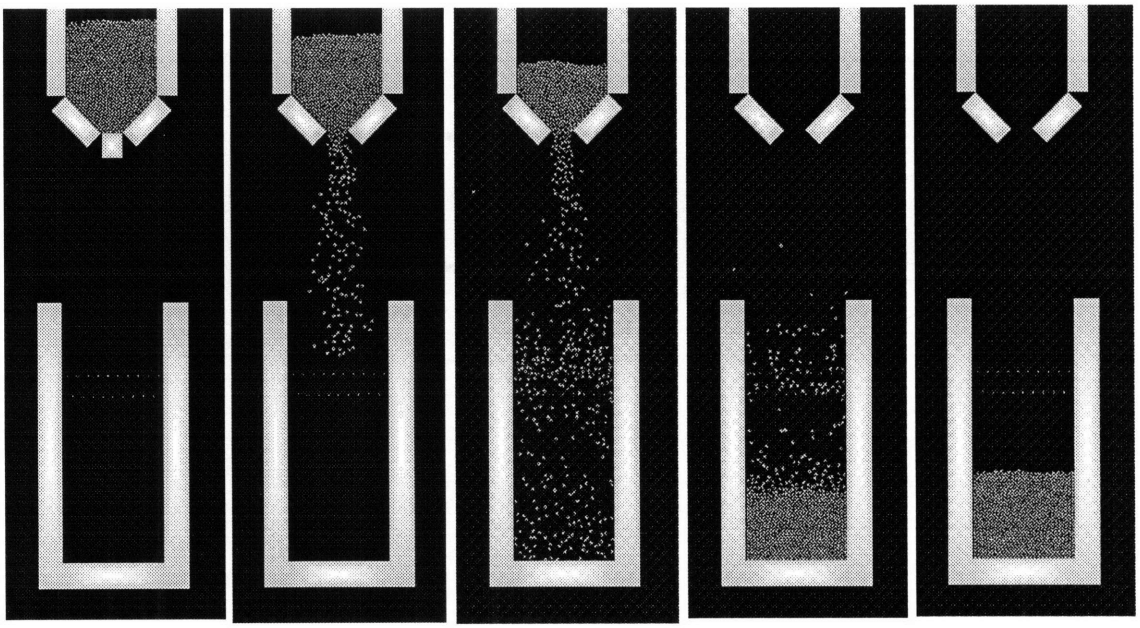

Figure 4.3: MSP Simulation (B) with Narrow Hopper Opening (20 mm)

Differences were also apparent with the change in the interparticle friction coefficient. When the coefficient was 0.5, the particles fell from the hopper more slowly, resulting in a reduced deposition intensity. With the 20 mm opening and 0.5 friction coefficient, it took

time for the first particles to fall, as the opening was plugged momentarily. Reducing the friction coefficient to 0.1 increased the flow rate from the hopper and eliminated the plugging.

4.3 Experimental Results

The final densities from each of the experiments are shown in Table 4.1. The density of the sample up to a height was determined by adding up the total area of particles up to that height and dividing by the total area (height times width of the mold). The values shown in the table are the average values of the densities up to the centers of 200 of the particles above the center of the deposit. The values do not identify local heterogeneities, but provide a meaningful comparison of the average densities of the different samples. The final column presents an approximation of relative density using the following equation similar to Equation 2.4:

$$RelativeDensity = \frac{D - D_{min}}{D_{max} - D_{min}} \tag{4.1}$$

D is the density (% solids) of the sample and D_{max} and D_{min} are the maximum and minimum densities obtained in this series of experiments. Each simulation has been given an identifying letter to allow for discussion of comparisons.

4.4 Influence of Experimental Variables

As shown in Table 4.1, eight simulations were run for each pair of variables in which all other parameters were held constant. This creates eight different comparisons of the effect of each variable. Figures 4.4 to 4.7 show bar graphs comparing the densities resulting from the different changes. Only two values were tested for each variable (e.g., two heights), but preliminary experiments showed that these values could adequately display the expected changes in behavior resulting from that variable or that they were the extreme

values that could be used in the simulations. In the case of the drop height, any value above 800 mm would have required a smaller timestep due to the increased speed of fall from the greater heights. When the falling particles collided with the sieve wires at high speeds, the particles and the wires overlapped significantly. This overlap resulted in much greater forces on the particles which often shot off in random directions indicating that the soft contact model did not adequately model the behavior with the timestep being used.

Simulation	Hopper Opening (mm)	Drop Height (mm)	Interparticle Friction Coefficient	Presence of Sieves	Final Density (% solids)	Relative Density (%)
A	20	400	0.1	No	90.061	100.0
B	20	400	0.1	Yes	89.737	90.8
C	20	400	0.5	No	88.767	63.3
D	20	400	0.5	Yes	88.423	53.6
E	20	800	0.1	No	89.703	89.9
F	20	800	0.1	Yes	89.667	88.8
G	20	800	0.5	No	88.867	66.2
H	20	800	0.5	Yes	88.714	61.8
I	40	400	0.1	No	89.131	73.6
J	40	400	0.1	Yes	89.527	84.9
K	40	400	0.5	No	86.771	6.8
L	40	400	0.5	Yes	87.614	30.7
M	40	800	0.1	No	89.991	98.0
N	40	800	0.1	Yes	89.368	80.4
O	40	800	0.5	No	86.532	0.0
P	40	800	0.5	Yes	87.567	29.3

Table 4.1: Final Densities of Sixteen MSP Simulations

Hopper Opening

Figure 4.4 shows a comparison of the simulations where the width of the hopper opening was varied. In seven of the eight cases, the smaller hopper opening resulted in a greater density of the sample. The effect is more pronounced in the simulations with the higher friction coefficient value (0.5). This behavior is in agreement with the observation in physical experiments that a reduction in deposition intensity increases the final density of the sample.

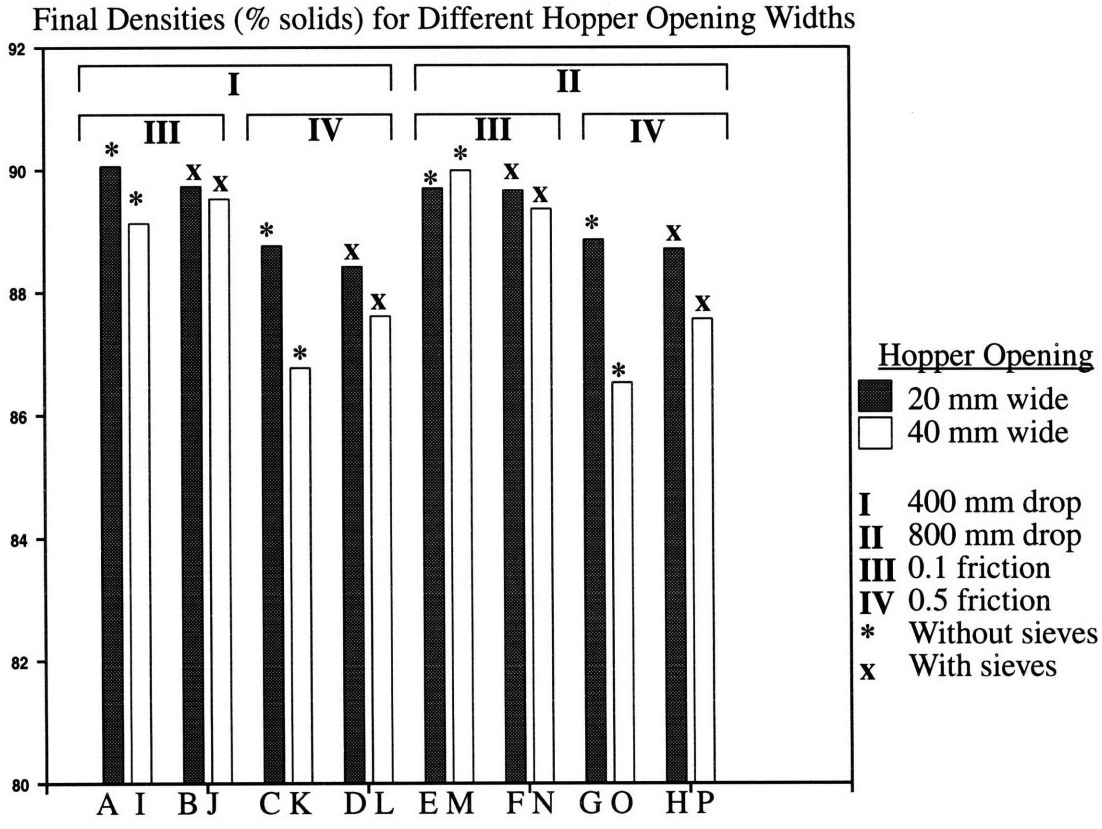

Figure 4.4: Comparison of Densities of Simulations with Narrow and Wide Hopper Openings

Drop Height

Varying the drop height did not have consistent effect on the final sample densities. Figure 4.5 shows that the 800 mm drop height increased the density of the sample in only three of the eight cases and the range of variation was highly variable. One explanation for this behavior is that the range of values tested might not be large enough, however these were the practical limits as described previously. The effects of the drop height also might be affected by the constant drop height between the bottom of the sieves and the receiving mold.

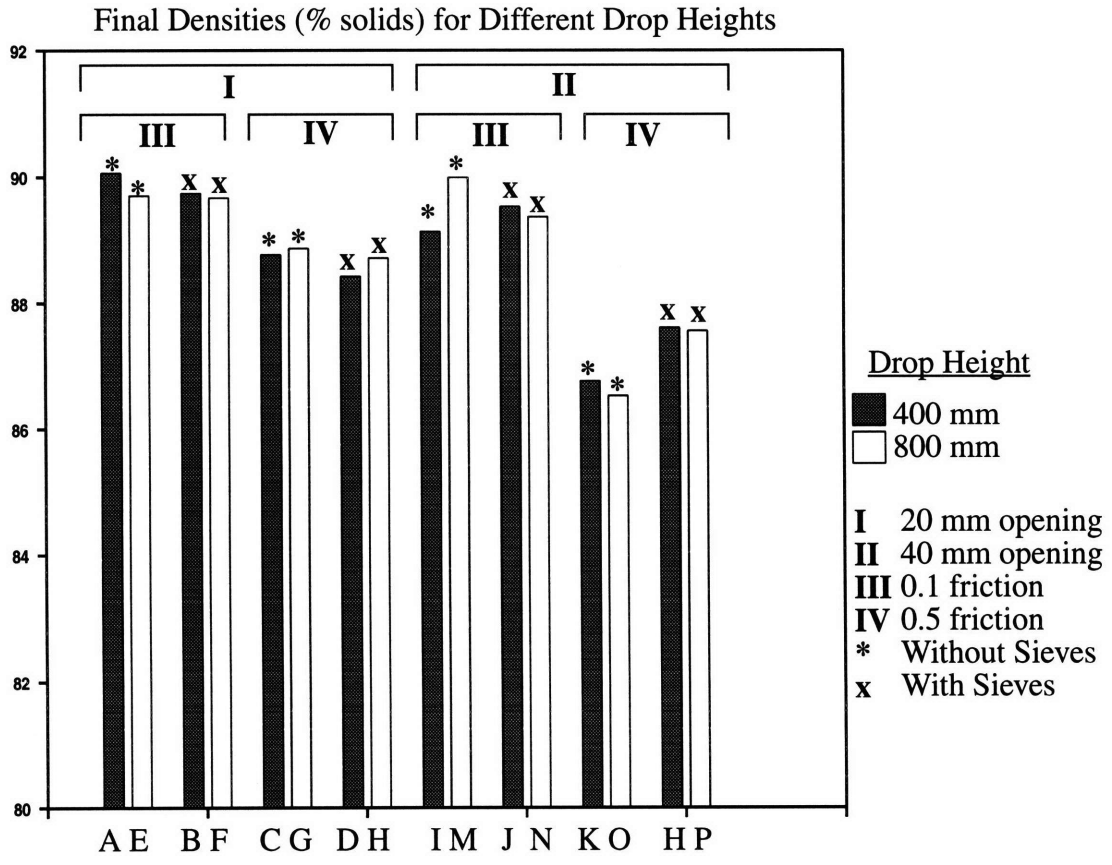

Figure 4.5: Comparison of Densities of Simulations with Different Drop Heights

Interparticle Friction

The interparticle friction coefficient had the greatest effect of all of the simulation variables on the final density of the pluviated samples. In all cases, there was a significant decrease in the density when the interparticle friction coefficient was increased from 0.1 to 0.5. While the increased friction should have decreased the deposition intensity of the flow from the hopper, it also increased the shear force between the particles after they had settled in the hopper. This enabled behavior such as arching to protect voids in the sample. The right half of the figure shows that the wider hopper opening magnified this effect.

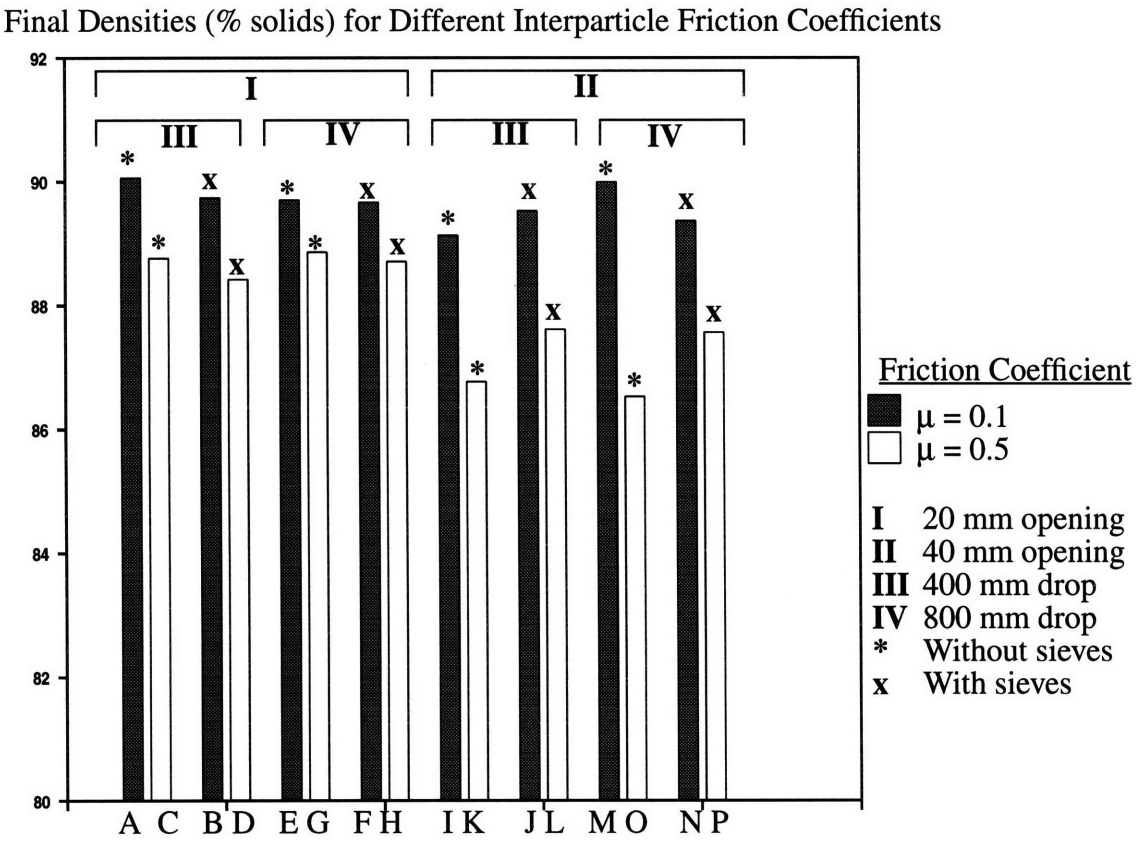

Figure 4.6: Comparison of Densities of Simulations with High and Low Interparticle Friction Coefficients

Presence of Sieves

The presence of sieves did not have the same effect on the density for all of the simulations. A comparison of the results of changing this variable is shown in Figure 4.7. In five of the cases the presence of the sieves decreased the final density, while the other three had an increase. In theory, the addition of the sieves would increase the level of particle interference and thus reduce the density (Lo Presti et al. 1992).

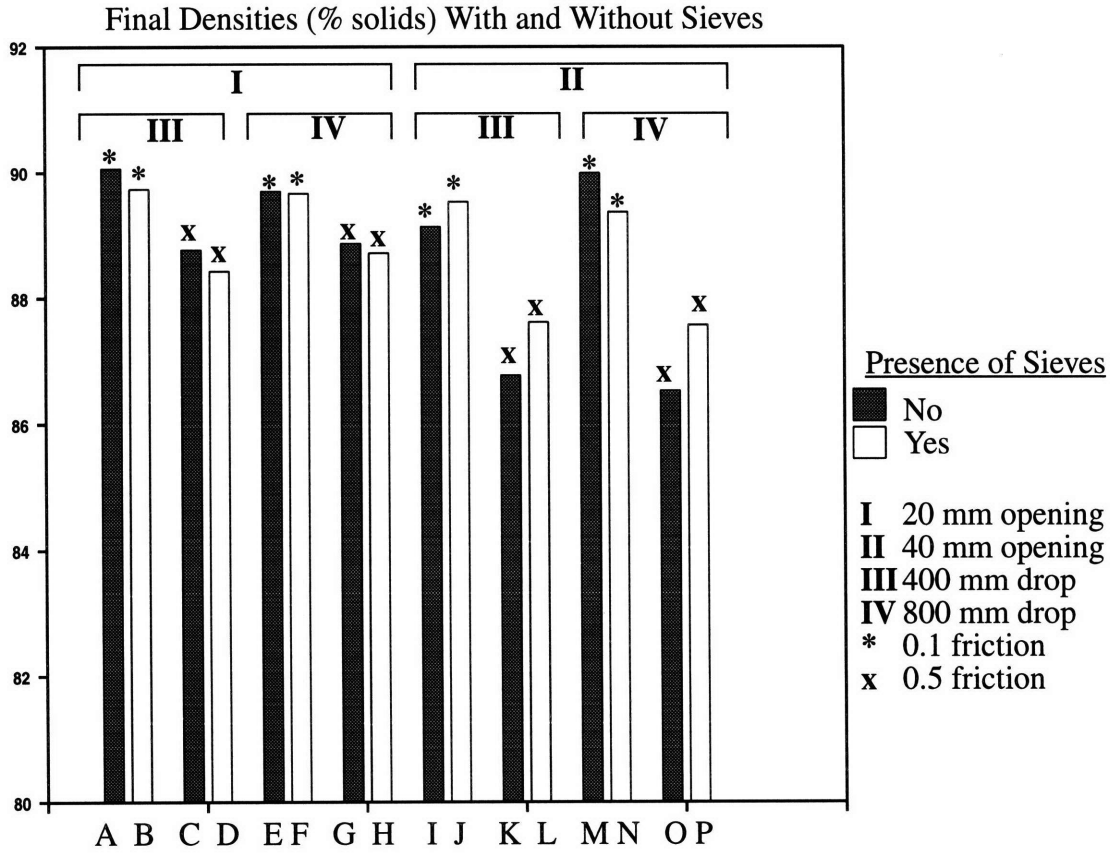

Figure 4.7: Comparison of Densities of Simulations With and Without Sieves

4.5 Removal of Particles

While changing the variables in the MSP simulations did exhibit the expected behavioral trends, other methods were necessary to obtain a greater range of densities. To simulate Ladd's (1997) proposed process of including sugar or salt in the particle mixture and dissolving them with water, particles were removed from the settled assembly. MIMES allows for the deletion of a particle without disruption of neighboring particles. After a sample was prepared using MSP simulations, up to eighty particles were removed from the sample. The sample was then subjected to its own weight until it had reached a new equilibrium configuration.

When a particle was removed, there was either a slight shift in the surrounding particles or a local collapse to fill the void. In the samples with an interparticle friction coefficient of 0.1, almost all voids collapsed under the weight of the above particles. Since this procedure did not produce significant reductions in density, it was abandoned. The samples with an interparticle friction coefficient of 0.5 were able to support the gravity loads more successfully even though there was increasing settlement as more particles were removed. Removing more than eighty particles (ten percent of the sample) did not bring about significant decreases in sample density.

After the particle removal process, the majority of the remaining grains maintained their same general orientation. This indicates that aside from the artificial voids the samples retained the "natural" fabric created from the pluviation. These samples were then used in the compression and shear experiments described in the following two chapters.

Chapter 5

One-Dimensional Compression Simulations

5.1 Experimental Program

The second set of experiments modeled one-dimensional compression tests, also known as oedometer tests. Samples of different densities were prepared in a fixed mold and compressed downward by a rigid plate moving at a constant velocity. The forces on the walls of the mold and the top plate were recorded over time and the stress-strain behavior of the samples was determined.

After the samples of the granular material were placed in the receiving mold using Multiple Sieve Pluviation (similar to method L in Table 4.1) and the particle removal process described in Section 4.5, they were further prepared for the oedometer tests. The particles on the top surface of the sample were rearranged to create as level a surface as possible. A very light horizontal plate was then suspended slightly above the top surface of the sample and allowed to descend under gravity onto the particles. Rotation and horizontal motion of this plate were prevented as it came to rest atop the sample. The top plate was made of a material with a density that was one percent of the density of the particles to ensure that its weight did not affect the granular assembly when it settled. After pluviation, the sample was about 90 mm in height, which is the height to which the top plate settled. All particles in these experiments had an interparticle coefficient of friction of 0.5 and the Rayleigh damping constant was 300 as described in Chapter 3. The mold walls were made frictionless to prevent side effects during the vertical deformation. The top plate velocity was 10 mm/s and the time step was again 5×10^{-5} seconds.

Before the compression was started, the densities of the samples were measured by dividing the area of solids by the total area in the mold. This includes voids at the top sur-

face of the sample and gives slightly lower density values than those calculated for the MSP simulations in Chapter 4. Table 5.1 shows the initial packing fractions and void ratios for each of the simulations.

Particles Removed	Initial Packing Fraction(%)	Initial Void Ratio (e_0)
0	85.07	0.176
20	82.94	0.206
40	81.27	0.230
80	78.89	0.268

Table 5.1: Initial Densities of Samples in One-Dimensional Compression Simulations

For each simulation, the forces, displacements, and velocities in the horizontal, vertical, rotational directions were tracked for the top plate and the bottom and side walls. From these values, the vertical strain, vertical stress, horizontal stress, and the coefficient of earth pressure at rest were calculated. The stresses are reported as force divided by distance since the simulation occurs in a plane. The vertical strain is calculated as the change in height of the sample (h) divided by the original height (h_0):

$$\varepsilon_v = \frac{\Delta h}{h_0} = \frac{h - h_0}{h_0} \tag{5.1}$$

The vertical stress is calculated as the average of the force on the top and bottom plates divided by the original cross-sectional width (w_0) which remained constant:

$$\sigma_v = \frac{F_{top} + F_{bottom}}{2w_0} \tag{5.2}$$

The horizontal stress had to be calculated with the changing height of the sample as:

$$\sigma_h = \frac{F_{right} + F_{left}}{2h} \tag{5.3}$$

where the height is constantly decreasing as the top plate moves down. The coefficient of earth pressure at rest (K_0) is the ratio of the horizontal stress to the vertical stress:

$$K_0 = \frac{\sigma_h}{\sigma_v} \tag{5.4}$$

Equation 2.4 then relates K_0 to friction angle of the soil.

Force measurements in Discrete Element simulations with a large number of bodies tend to oscillate from one timestep to the next, resulting in wide bands on plots of data. While this information is significant in understanding the behavior of the Discrete Element simulation, it is not of interest when considering the behavior of the system being modeled. For this reason, data was smoothed when plotting results. Each value on the graphs is the average of the values from the 50 previous timesteps and the next 50 timesteps. Smoothing was not done until the final results were calculated. Values for vertical stress, horizontal stress, vertical strain, and K_0 were all smoothed using this process. This results in much clearer plots of the data shown later in this chapter.

The variable used for these simulations was the initial density of the sample. All of the simulations started with the same initial sample created using pluviation. Zero, twenty, forty, and eighty particles were removed from the sample for the four experiments. After particle removal, there was slight settlement of the samples under their own weight, but they maintained more or less the same fabric as the original sample.

5.2 Behavior of Simulations

After the top plate had settled and come to rest, the simulation was started and the plate was forced down at a constant velocity. Series of four still frames are presented in Figures 5.1 and 5.2 showing the sample with zero particles removed and the sample with forty particles removed respectively. The frames are ordered from (a) to (d) with (a) being the initial state and (d) being the state immediately before the sample "exploded" as described below. In both cases, the initial strain is mostly due to rearrangement of the particles at the top surface of the sample. This is similar to seating that occurs in physical

experiments. As more particles come into contact with the top plate, the force is distributed more evenly through the sample and the strain is more uniform.

It can be seen in Figure 5.1 that as the sample compresses, the general structure of the sample with zero particles removed does not change that much. Figure 5.2 shows a different behavior as particles shift to fill in the voids resulting in new rotations and contacts for many of the particles. Figure 5.2(d) shows that the majority of the voids have disappeared from the sample by the time the simulation ended.

The simulations were stopped when the assembly exploded, sending particles outside of the mold. This is a result of the timestep being too large for the magnitude of forces generated between particles. To extend the simulation beyond that point it would be necessary to reduce the timestep. However to truly model the behavior at such large strains, it would be necessary to account for particle crushing.

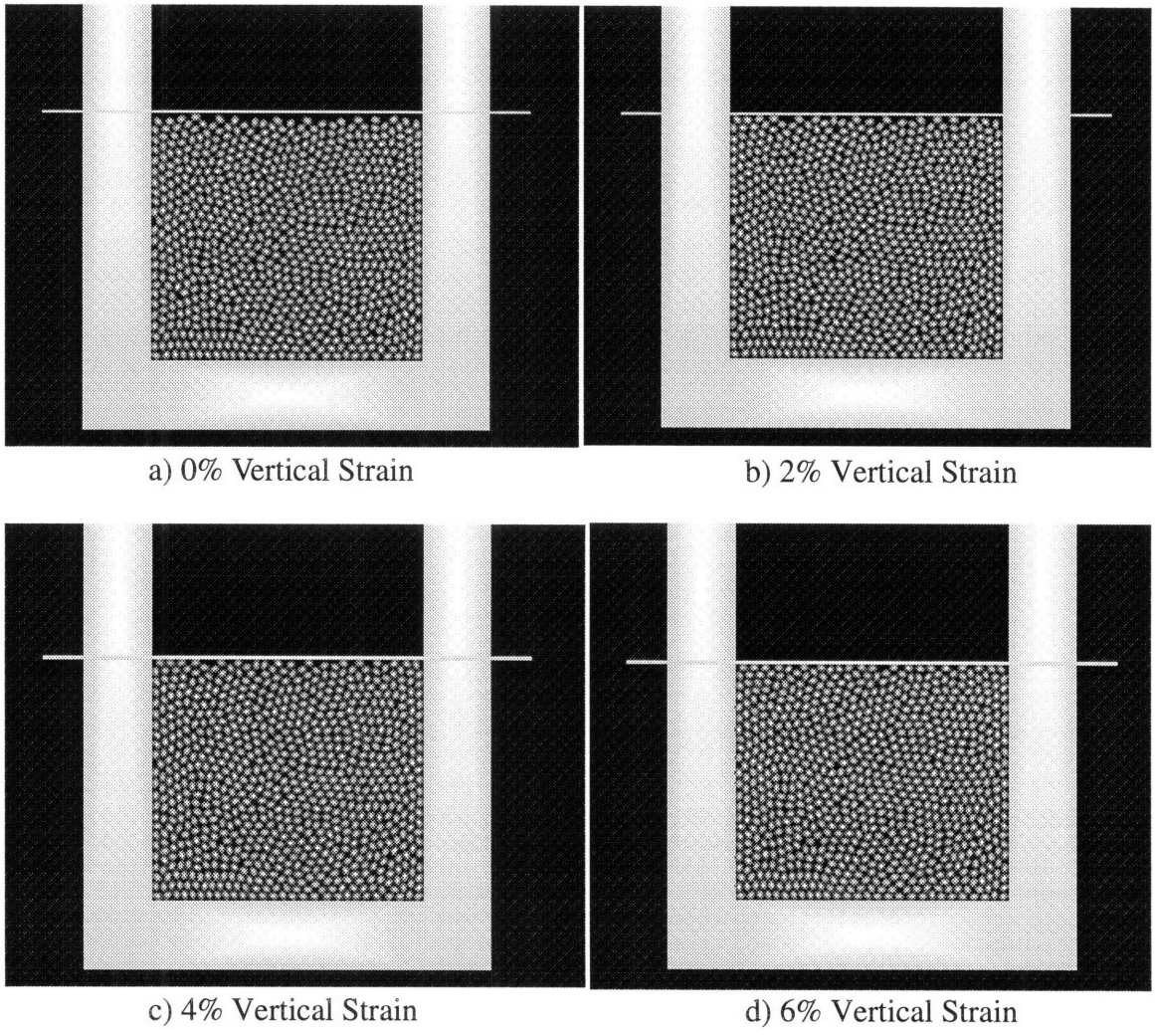

a) 0% Vertical Strain

b) 2% Vertical Strain

c) 4% Vertical Strain

d) 6% Vertical Strain

Figure 5.1: One-Dimensional Compression Test of Sample with Zero Particles Removed

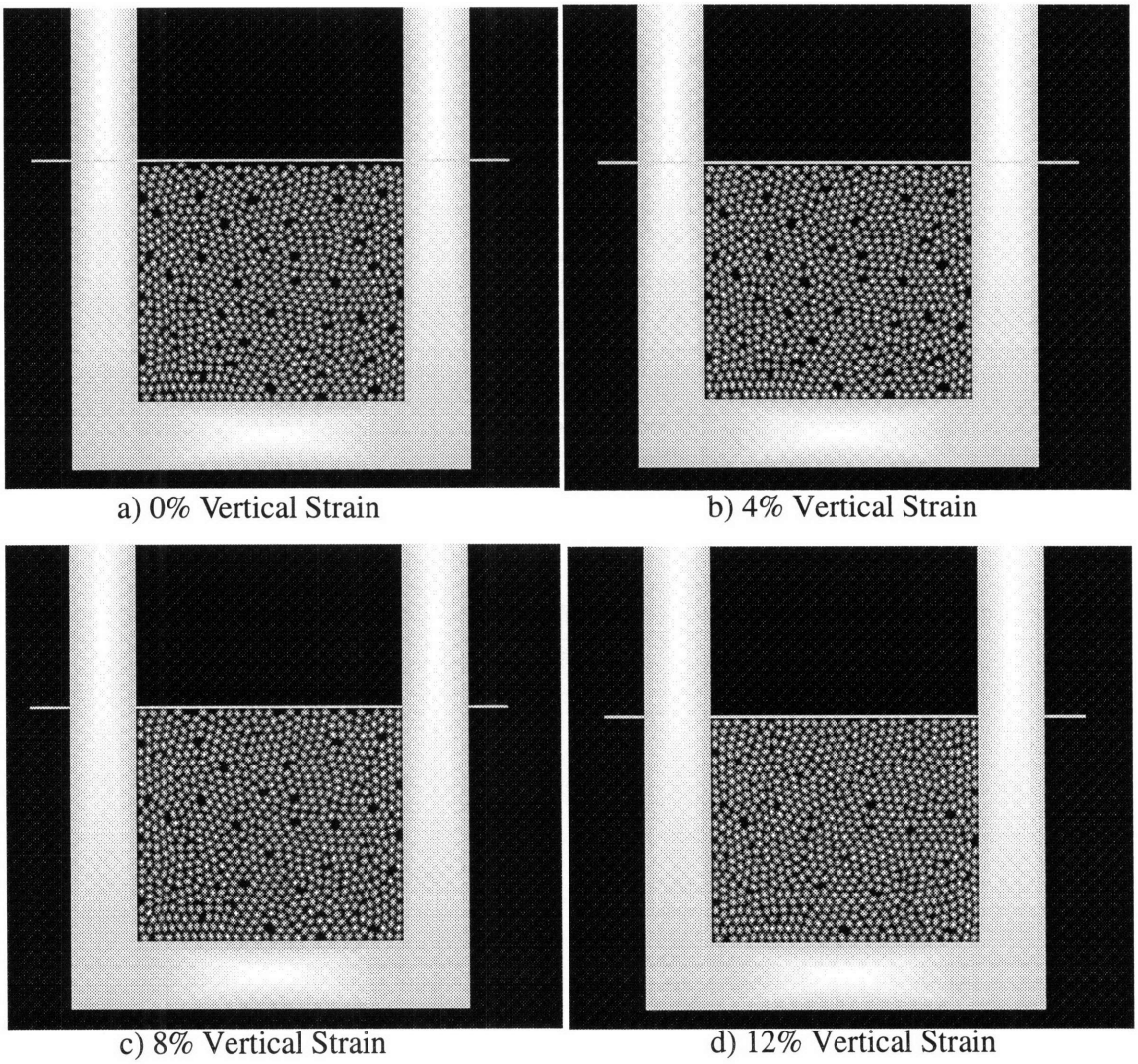

a) 0% Vertical Strain

b) 4% Vertical Strain

c) 8% Vertical Strain

d) 12% Vertical Strain

Figure 5.2: One-Dimensional Compression Test of Sample with Forty Particles Removed

5.3 Experimental Results

For each simulation, four different graphs were prepared. Figures 5.3-5.6 show the plots for the four simulations. Comparisons of the cases are discussed in the next section. For each case, graph (a) plots the vertical strain versus the vertical stress. The stress starts slightly above zero because of the self-weight of the particles. The initial vertical portion of the graph is a result of seating at the top of the sample. This corresponds with the visual observations in Figures 5.1 and 5.2. After that portion, there is a linear region in which the stress increases proportional to the strain. This region is when the rearrangement of particles takes place. Finally, the graph turns concave as the resistance to rearrangement grows and some of the displacement comes from the deformation of the contact springs between the particles. Graph (b) shows the same data with stress on a log scale. This plot shows a clear transition from the point of seating. The same general behavior is observed in all four cases.

The other two graphs display the relationship between the vertical and horizontal stresses. Graph (c) plots the horizontal stress versus the vertical stress. Again, both values start above zero because of the self-weight of the particles. There is a nearly linear relationship between the two stresses. This is displayed in Graph (d) where the ratio of the horizontal stress to the vertical stress, K_0, is plotted against vertical stress. K_0 is the secant slope of Figure 5.3c. In general, there is a slight increase in K_0 with increasing vertical stress.

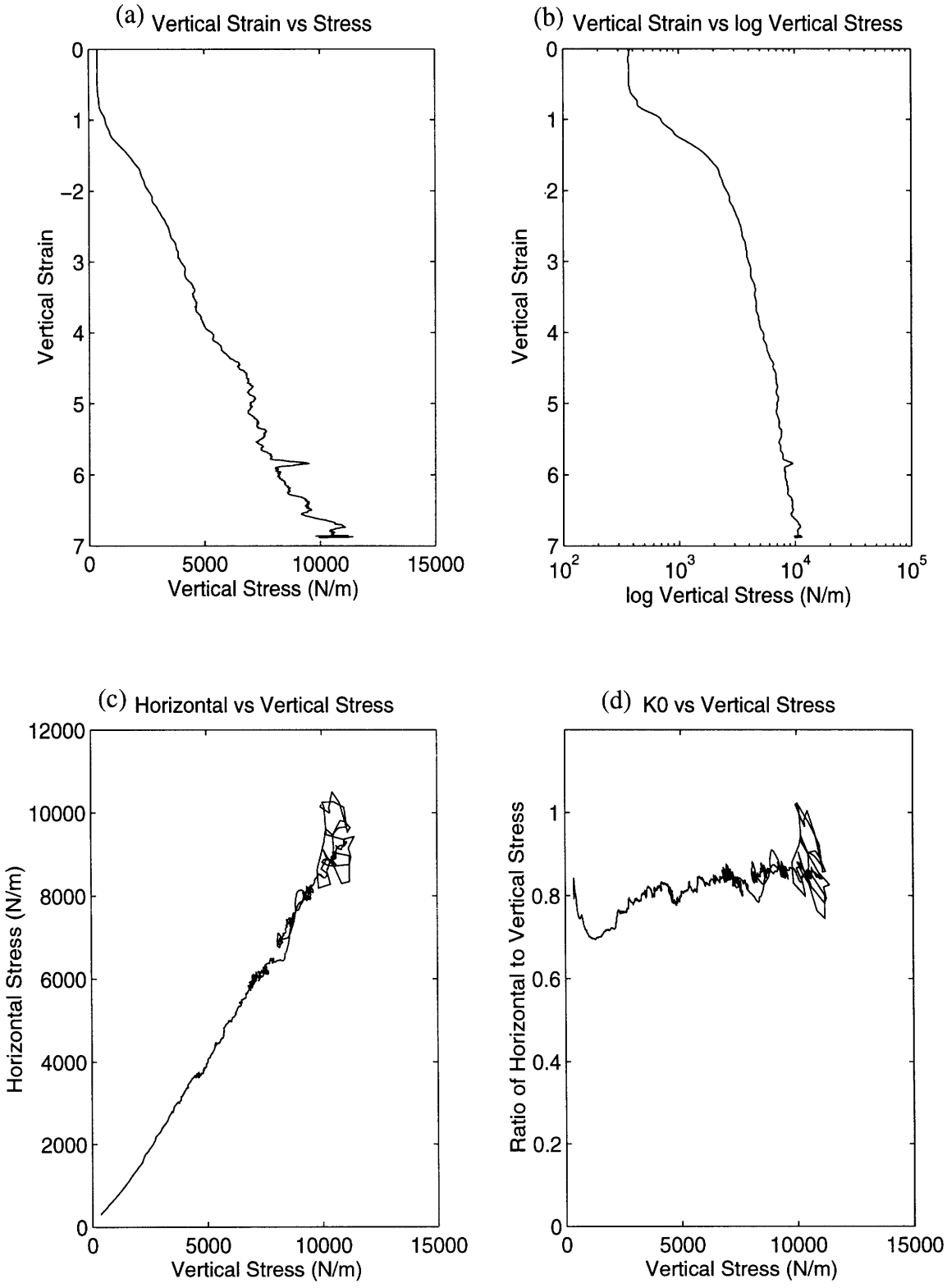

Figure 5.3: One-Dimensional Compression Test Results - Zero Particles Removed (e_0=0.176)

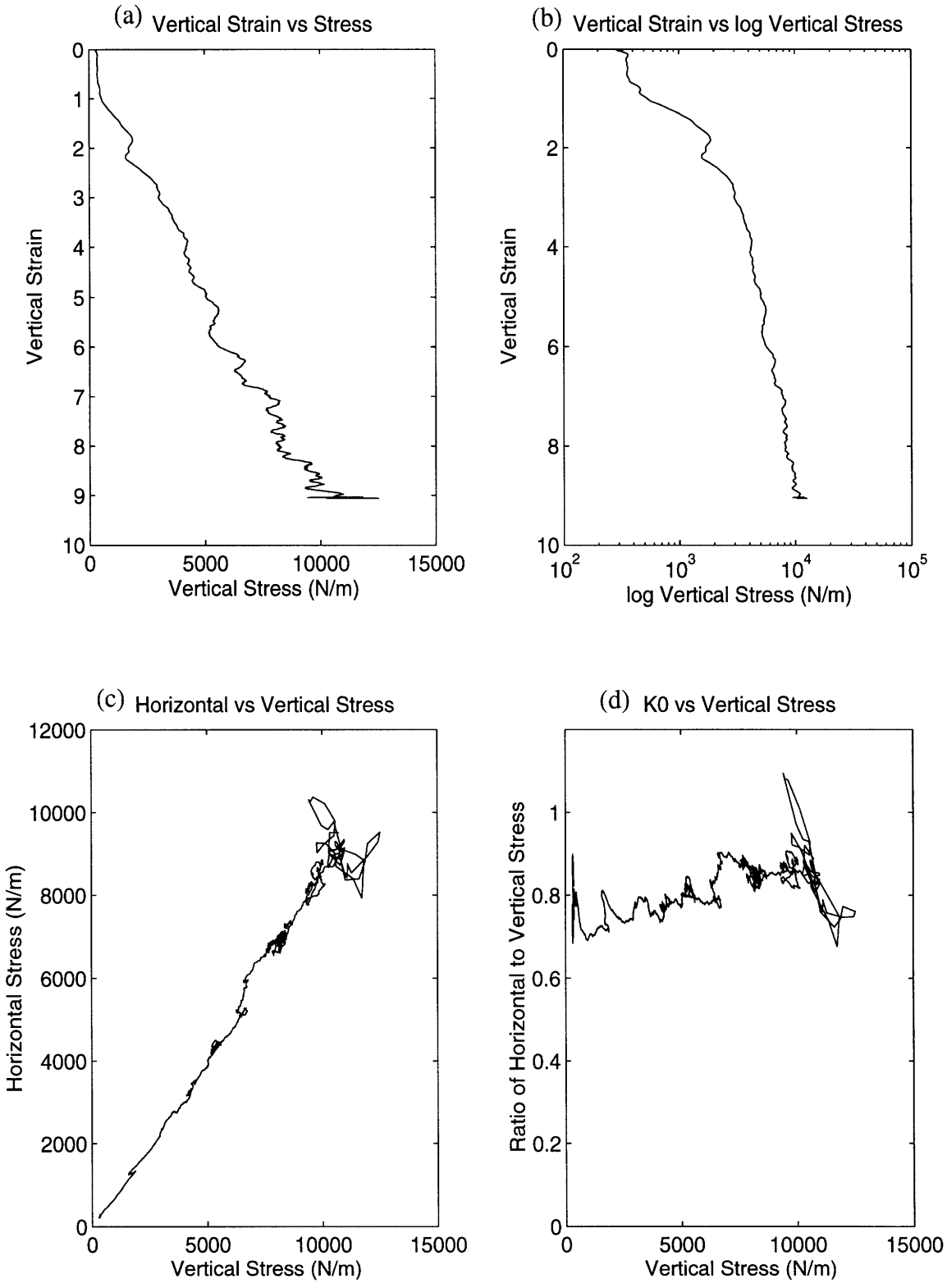

Figure 5.4: One-Dimensional Compression Test Results - Twenty Particles Removed (e_0=0.206)

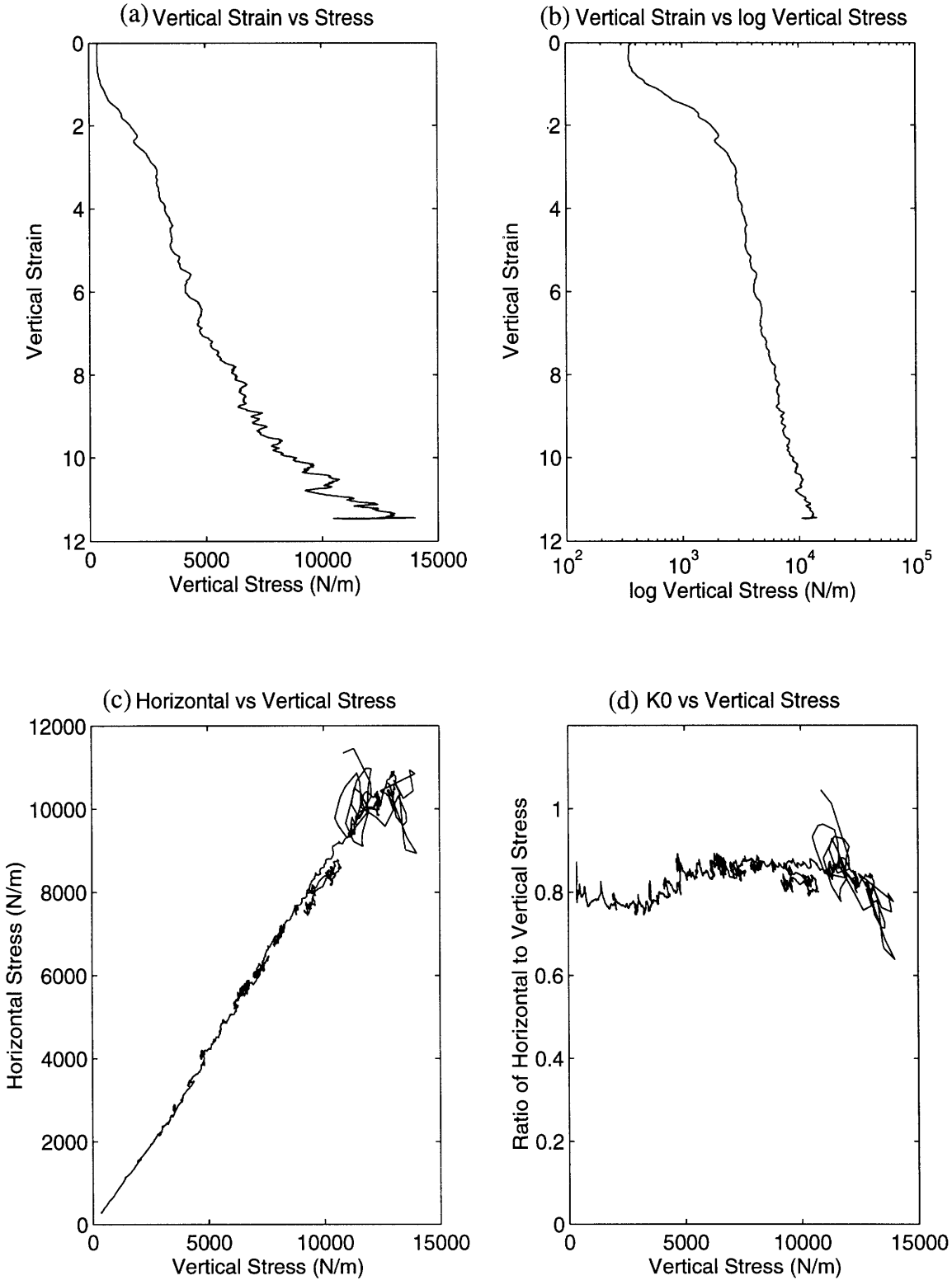

Figure 5.5: One-Dimensional Compression Test Results - Forty Particles Removed (e_0=0.230)

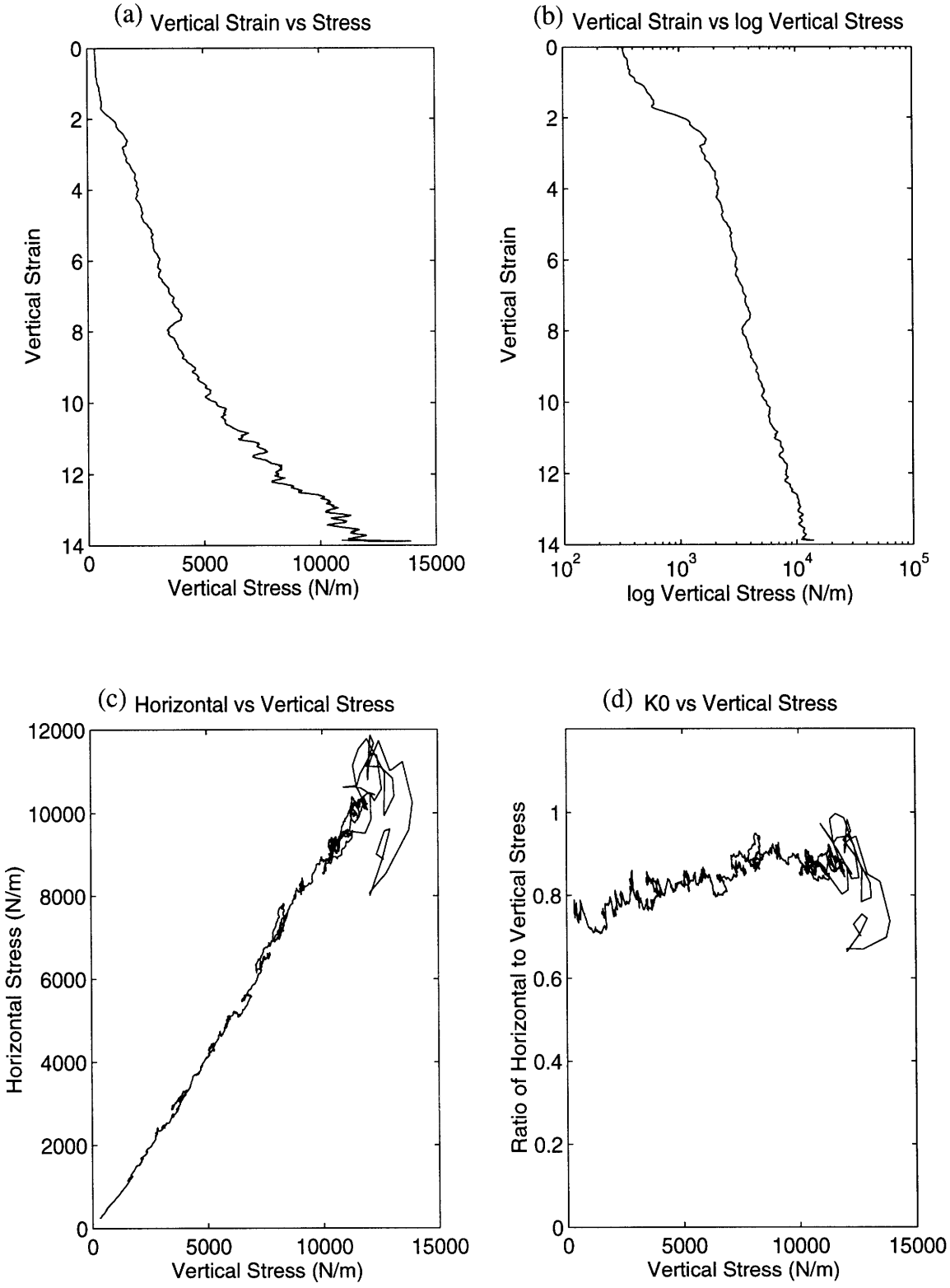

Figure 5.6: One-Dimensional Compression Test Results - Eighty Particles Removed (e_0=0.268)

5.4 Effect of Initial Density

The experiments all show that initial density has a major effect on the stress-strain behavior of one-dimensional compression tests of granular materials. A plot of the vertical strain versus vertical stress for samples with different initial densities is shown in Figure 5.4. This graph shows that the change in vertical strain during seating is almost the same for all of the cases. The four plots then differ within the linear range. Table 5.2 shows the constrained modulus (inverse slope = stress/strain) of the four tests in the linear range. The constrained modulus increases as the density of the sample increases. This is explainable because the reduction in voids leaves less unstable voids for particle rearrangement, which is the cause of the initial deformation under low stress..

Particles Removed	Stress Range in Linear Region (N/m)	$(d\sigma_v/d\varepsilon_v)$ in Linear Region (N/m)/(%strain)	Average K_0 in Linear Region
0	500-6000	1650	0.781
20	500-5500	1150	0.756
40	500-5000	700	0.792
80	500-4000	500	0.775

Table 5.2: Data from Linear Region of One-Dimensioal Compression Stress-Strain Plots

The reduction in voids also reduces the maximum strain before the graph turns concave. The larger number of voids leaves a greater space for compression during the rearrangement phase. Table 5.2 shows the limits of the stress range for the linear region in each plot. The maximum stress in the linear region is higher for the denser samples. There is also a more gentle transition from the linear region into the concave region.

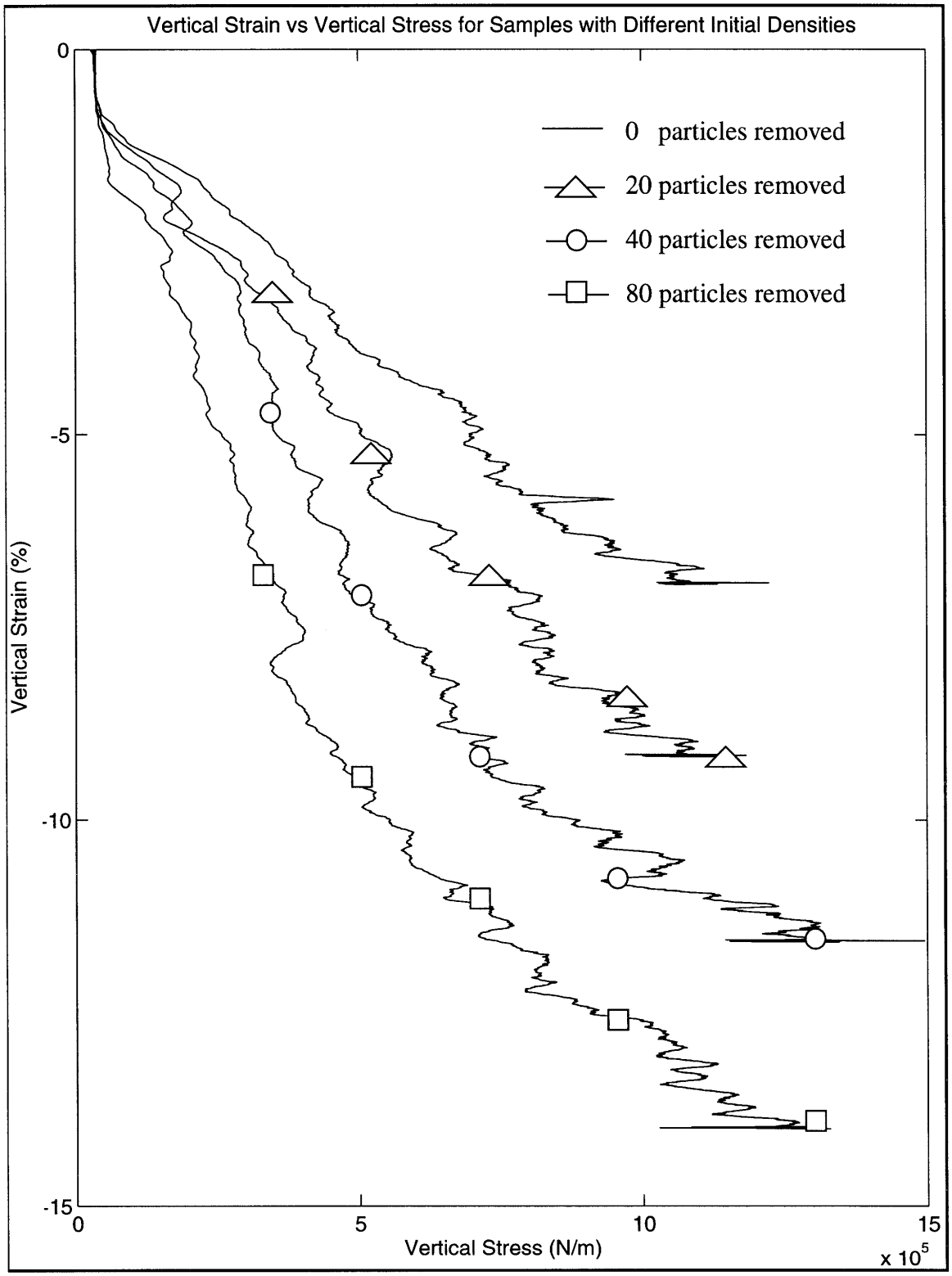

Figure 5.7: One-Dimensional Stress-Strain Behavior for Different Initial Densities

The K_0 value for all of the simulations starts slightly below 0.8 and tends to increase with increasing stress. Table 5.2 shows average values of K_0 in the linear range of the graphs. This indicates that the density does not significantly affect K_0. From equation 2.4 ($K_0 = 1 - \sin \phi$), the corresponding friction angles (ϕ) for these assemblies range from 12.0 to 14.1 degrees, which are very low. Typical values of K_0 for sands are about 0.4 or 0.5 for friction angles of 30 to 35 degrees. The friction angle found here will be compared with the friction angles from triaxial compression tests described in Chapter Six.

It is also worth noting that all of the simulations ended at about the same final density. Table 5.3 shows the final density and void ratio of the samples before they "exploded".

Particles Removed	Final Packing Fraction(%)	Final Void Ratio (e_0)
0	91.36	0.095
20	91.21	0.096
40	91.79	0.089
80	91.62	0.091

Table 5.3: Final Densities of Samples in One-Dimensional Compression Simulations

Chapter 6

Drained Triaxial Compression Simulations

6.1 Experimental Program

The final set of experiments simulated drained triaxial compression tests sheared at constant lateral confining stress. Samples with different initial densities were prepared in a mold as in the one-dimensional compression tests. For each simulation, the samples were compressed one-dimensionally to the desired level of horizontal stress. This confining stress was applied to the sample and was held constant for the remainder of the simulation. At this point, the side walls were released to move horizontally, but the horizontal force was varied to maintain a constant confining stress during shear. All material parameters and initial apparatus dimensions were the same as in the one-dimensional compression simulations. The simulations were run to twenty percent vertical strain if possible.

After compressing the samples to the desired level of confining pressure, the densities of the samples were measured as described in Chapter 5. Table 6.1 shows the initial packing fractions and void ratios for each of the simulations

Particles Removed	Confining Pressure (N/m)	Initial Packing Fraction(%)	Initial Void Ratio
0	572	87.31	0.145
0	1148	87.49	0.143
0	2319	88.07	0.135
40	579	83.61	0.196
40	1165	83.92	0.192
40	2369	84.99	0.177

Table 6.1: Initial Densities of Series of Triaxial Compression Simulations

For each experiment, the forces, velocities, and displacements in the horizontal, vertical and rotational directions at each time step were tracked for the plate and walls just as in the one-dimensional tests. Along with the horizontal and vertical stresses and vertical strains, the horizontal and volumetric strains and the ratio of vertical stress to horizontal stress were calculated. The vertical strain and horizontal stress were calculated using Equations 5.1 and 5.3 respectively, but the calculation for the vertical stress had to reflect the changing width of the sample (w), so it was calculated as:

$$\sigma_v = \frac{F_{top} + F_{bottom}}{2w} \tag{6.1}$$

The horizontal strain was determined with the changing width also:

$$\varepsilon_h = \frac{\Delta w}{w_0} = \frac{w - w_0}{w_0} \tag{6.2}$$

The two-dimensional volumetric strain was measured based on the change in area:

$$\varepsilon_{vol} = \frac{A - A_0}{A_0} \tag{6.3}$$

Due to experimental limitations, the volumetric strain is often approximated by adding the one-dimensional strains, but MIMES allows for the calculation of the true value. In Equation 6.3, a zero volumetric strain does signify no change in volume from the original state.

The friction angle of the soil is calculated from the ratio R of the vertical stress to the confining stress:

$$R = \frac{\sigma_v}{\sigma_h} \tag{6.4}$$

This ratio is related to the friction angle ϕ of the soil by:

$$\sin\phi = \frac{R - 1}{R + 1} \tag{6.5}$$

The value for ϕ from this equation can be compared to the friction angle inferred from the one-dimensional compression tests, i.e, $K_0 = 1 - \sin\phi$ (Equation 2.4).

A different method was used to smooth the data than in Chapter Five so that there would be less fluctuation in the graphs. This was necessary to obtain values and slopes

from the plots. For these experiments, only one point was plotted for each 1000 time steps. The value at this point was the average value of the previous 500 timesteps and the following 500 timesteps. Again, smoothing was not done until the final values for presentation were calculated. The values that were averaged were the ratio of vertical stress to horizontal stress, the vertical strain, the volumetric strain, and the horizontal stress.

Six different simulations were run for the triaxial compression experiments. The two parameters varied were the initial density of the sample and the horizontal confining pressure. The densities used were the cases from the one-dimensional tests in which zero and forty particles were removed. For each of these, three different confining pressures were used. The first value was two times the horizontal stress resulting from the self-weight of the particles. This was the lowest value chosen because at lower values, the variation in stresses through the height of the sample did not adequately model the stress-strain behavior of the sample. This stress averaged about 570 N/m on both side walls. The other two values were approximately two and four times this minimum value, 1150 N/m and 2340 N/m.

6.2 Behavior of Simulations

As in the one-dimensional experiments, the vertical plate moved down at 10 mm/s when the simulation began. The sets of still frames in Figures 6.1 and 6.2 show the progression of the simulations for the sample with zero particles removed and the sample with forty particles removed, both at the lowest confining pressure. Again, the frames are ordered from (a) to (d) with (a) being the initial state after the desired level of confinement was reached (zero strain) and (d) being the twenty percent vertical strain level. The most noticeable difference from the one-dimensional compression tests is that freeing the horizontal walls allowed them to move outwards as the top plate came down. Another change

is that seating was not evident in the triaxial tests because the initial compression to achieve the desired confining stress eliminated this initial strain.

Both figures show that there is significant rearrangement of particles which was not as evident in the one-dimensional experiments. Figure 6.2 also shows that the initial voids introduced in preparing the sample disappear as the vertical strain is increased. By the time the samples had reached twenty percent vertical strain, they had changed their appearance almost entirely.

These simulations were capable of much greater strains than the one-dimensional compression simulations. As stated above, the simulations were all allowed to run until twenty percent vertical strain. In the one case with the highest confining stress and forty particles removed, the simulation became unstable as the forces between the particles and the side walls fluctuated too greatly before the end of the simulation as a result of the reduced number of particles in contact with the side walls. Consequently, the simulation was stopped at this point.

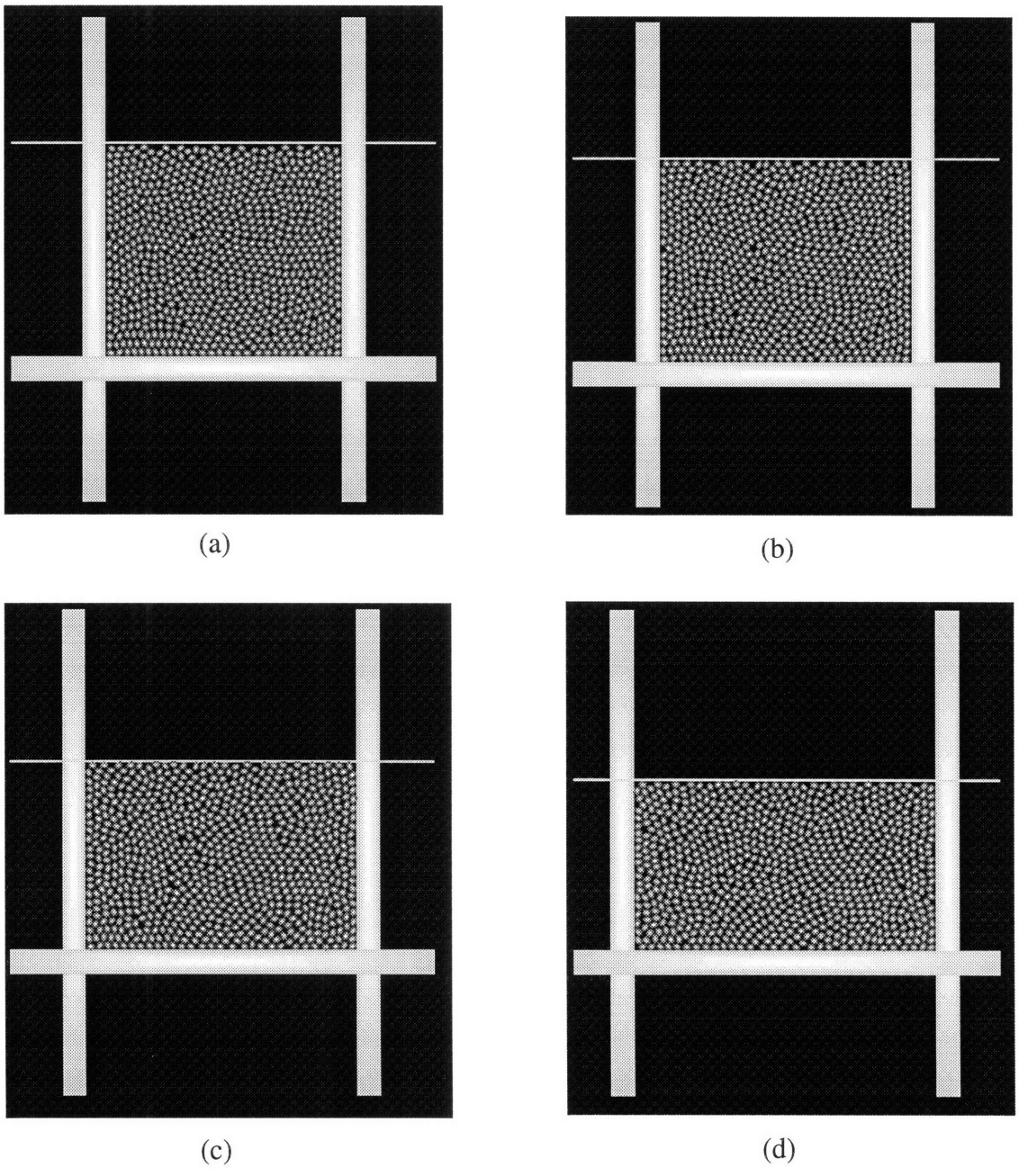

Figure 6.1: Triaxial Compression Test of Sample with No Particles Removed (Confining Stress = 572 N/m)

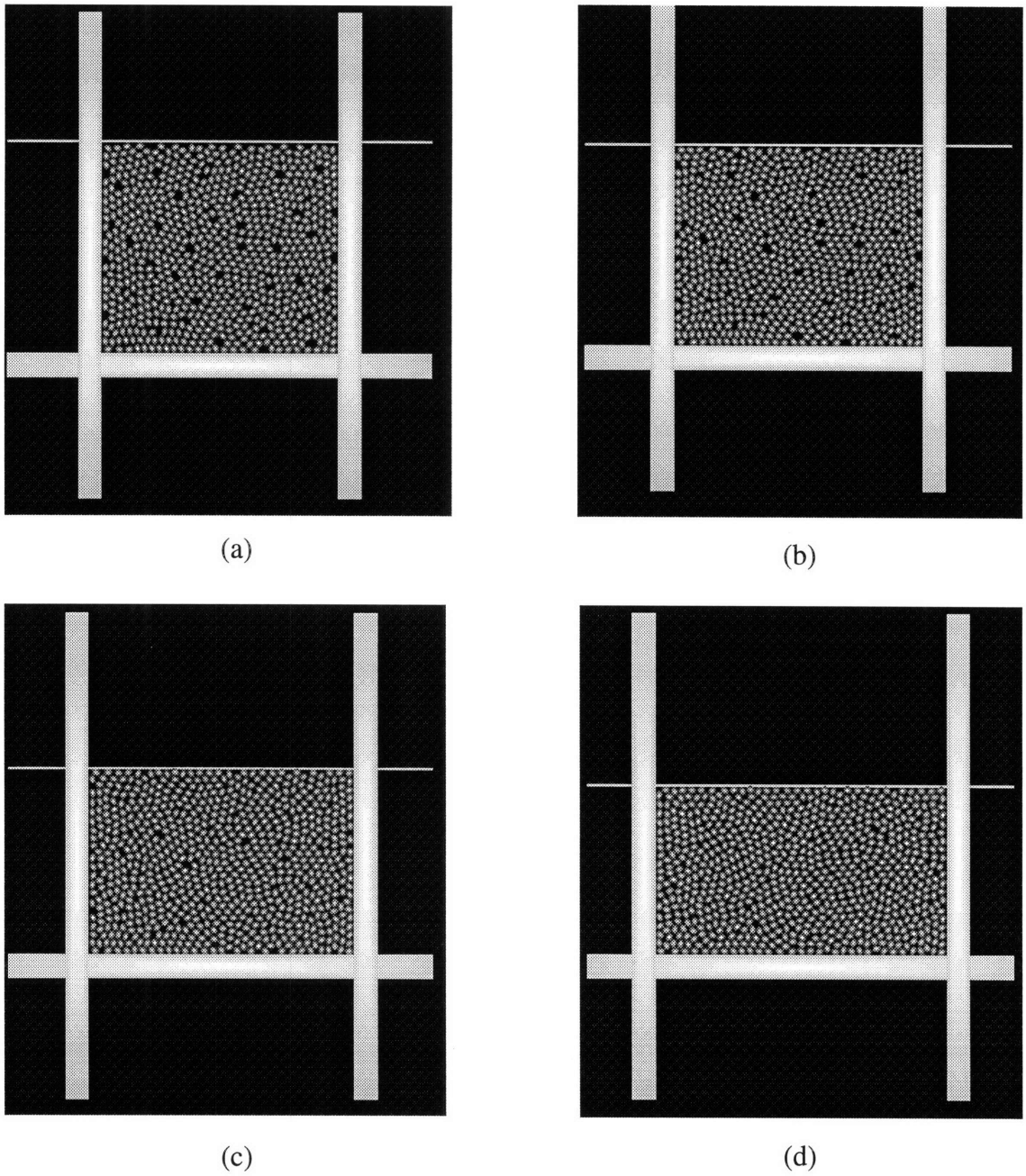

Figure 6.2: Triaxial Compression Test of Sample with Forty Particles Removed (Confining Stress = 579 N/m)

6.3 Experimental Results

Three plots were prepared for each simulation. Figures 6.3-6.8 at the end of this section show the plots for each of the cases. Comparisons of the cases with respect to initial density and confining pressure are in the next two sections. Graph (a) plots the ratio of the vertical stress to the horizontal stress versus the vertical strain. The vertical stress is normalized to show the relative effects of different confining pressures instead of the absolute effects as will be discussed in Section 6.5. Since the horizontal stress is constant, the shape of the curve will be the same in both cases. In this plot, there is an initial linear increase in the stress ratio much like in the one-dimensional experiments. However, unlike the one-dimensional case, a peak stress (failure) is reached after which strain softening is observed in some cases. This means that after shear failure, the sample has a lower resistance to shear. In the other cases, no softening occurs and the vertical stress remains approximately constant with increasing strain.

Graph (b) plots the volumetric strain versus the vertical strain. In all cases, the plot starts off with a negative slope, meaning that as the top plate initially moves down, the total volume of the sample decreases. However, the slope of the curve is increasing during shear, meaning that the rate of volumetric contraction is decreasing. In some cases, the curve reaches a minimum and then begins to rise, meaning that the sample is now expanding (i.e., it has a positive rate of dilation). It may reach its initial volume and show increasing dilation with continued shear. In other cases, no dilation occurs.

Graph (c) is included just to show that the horizontal stress is maintained at a constant value throughout the experiment. Although this data has also been smoothed, all graphs show that stress was successfully kept constant.

Tables 6.2 to 6.6 show various parameters obtained from the graphs. Since most of the plots are not very smooth, these data are approximations taken from the graphs by hand.

Table 6.2 displays values for the Young's modulus from the initial linear portion of the stress-strain curves (graph (a)). Since the vertical stress on that plot is normalized by dividing by the horizontal stress, the normalized Young's modulus is the slope of the curve in the linear region. This value is dimensionless. The actual Young's modulus of the sample is then obtained by multiplying by the confining stress. This value is shown in the last column.

Particles Removed	Confining Stress (N/m)	Normalized Young's Modulus (E/σ_h)	Young's Modulus (N/m)
0	572	61	34900
0	1148	36	41300
0	2319	19	44100
40	579	50	29000
40	1165	18	21000
40	2369	6.8	16100

Table 6.2: Young's Modulus Values of Triaxial Compression Simulations

Table 6.3 shows results at failure for the samples. This occurs at the peak stress ratio in each graph (a). The vertical strain at failure is also shown. The friction angle for the sand in each simulation is also calculated from Equation 6.5. The failure condition was somewhat difficult to identify in some of the graphs, since the stress ratio did not have a well-defined peak. This occurred in cases that gave the lowest friction angles.

Particles Removed	Confining Pressure (N/m)	Peak Stress Ratio/Stress	Vertical Strain at Failure(%)	Friction Angle
0	572	2.85/1630	6	28.7
0	1148	2.35/2700	7	23.8
0	2319	1.90/4410	8	18.1
40	579	2.25/1300	8	22.6
40	1165	2.00/2330	9	19.5
40	2369	1.90/4500	12	18.1

Table 6.3: Failure Point Data of Triaxial Compression Simulations

Table 6.4 show the rates of dilation obtained from graph (b). The rate of dilation is the slope of the graph and is a dimensionless quantity since it is a ratio of strains. A positive rate of dilation indicates that a sample is dilating, while a negative rate indicates that a sample is contracting. The third column shows the rate of dilation for each of the simulations at the yield point. The fourth column shows the maximum rate of dilation for the cases that experienced dilation. The final column shows the rate of dilation at the end of each simulation.

Particles Removed	Confining Pressure (N/m)	Failure Point Rate of Dilation	Maximum Rate of Dilation	Final Rate of Dilation
0	572	0.25	0.25	-0.095
0	1148	0.035	0.17	-0.050
0	2319	0.000	0.025	0.025
40	579	-0.135	-	-0.130
40	1165	-0.080	-	-0.020
40	2369	-0.140	-	-0.140

Table 6.4: Rates of Dilation of Triaxial Compression Simulations

Table 6.5 shows the densities of the samples at the ends of the simulations. These values were calculated in the same manner as those in Table 6.1. Again, both the packing fraction and void ratio are shown.

Particles Removed	Confining Pressure (N/m)	Final Packing Fraction(%)	Final Void Ratio
0	572	83.29	0.201
0	1148	86.22	0.160
0	2319	88.08	0.135
40	579	84.58	0.182
40	1165	85.87	0.165
40	2369	87.92	0.137

Table 6.5: Final Densities of Samples in Triaxial Compression Simulations

Finally, Table 6.6 shows the rates of strain softening in the cases in which strain softening was observed. The rate was calculated as the slope of graph (a) after failure. Again the rate is dimensionless as it is the dimensionless stress ratio divided by dimensionless strain.

Particles Removed	Confining Pressure (N/m)	Rate of Strain Softening (%)
0	572	-6.5
0	1148	-4.8
0	2319	-2.0

Table 6.6: Rates of Strain Softening of Triaxial Compression Simulations

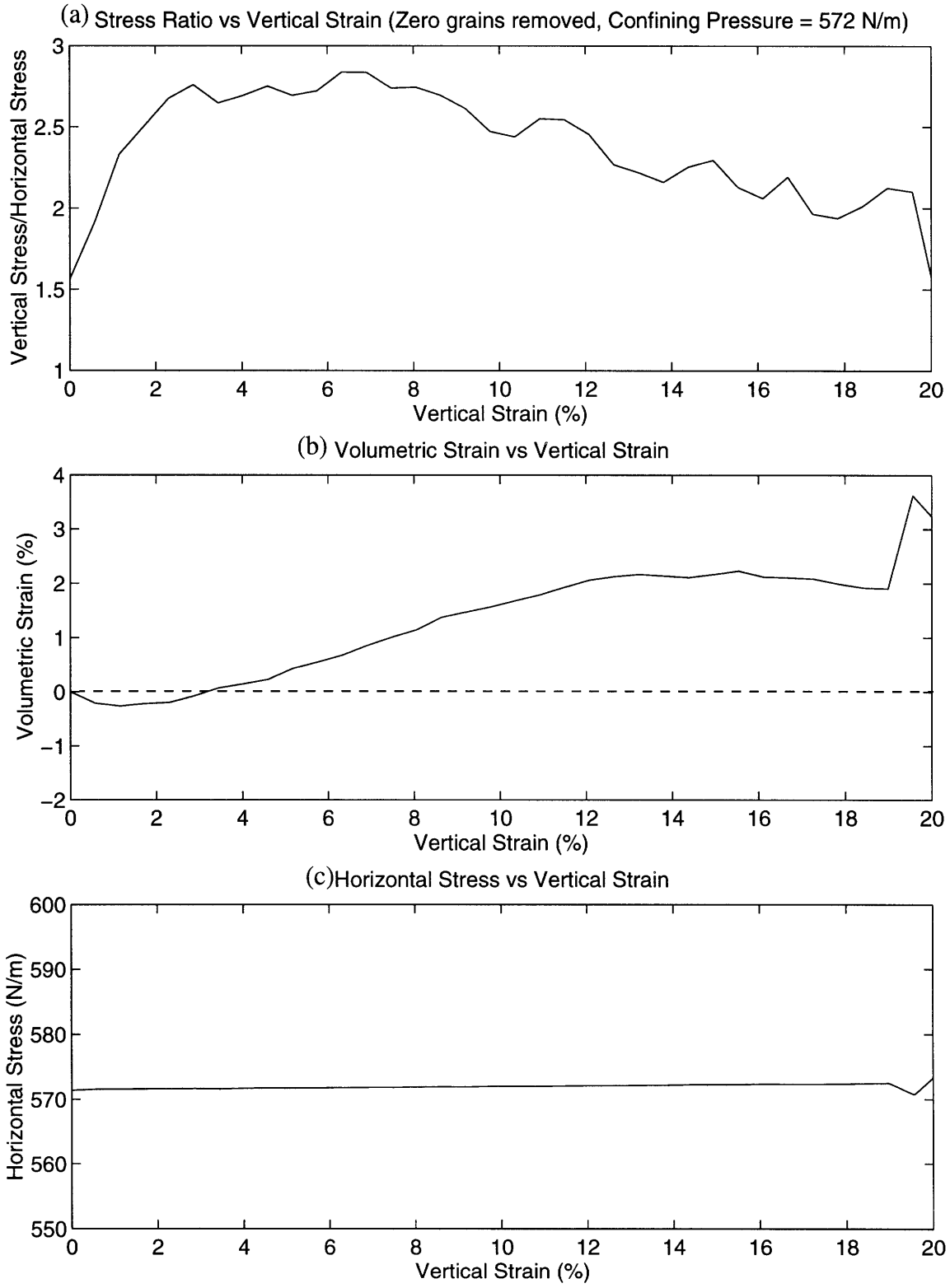

Figure 6.3: Triaxial Results - Zero Particles Removed, Confining Pressure = 572 N/m

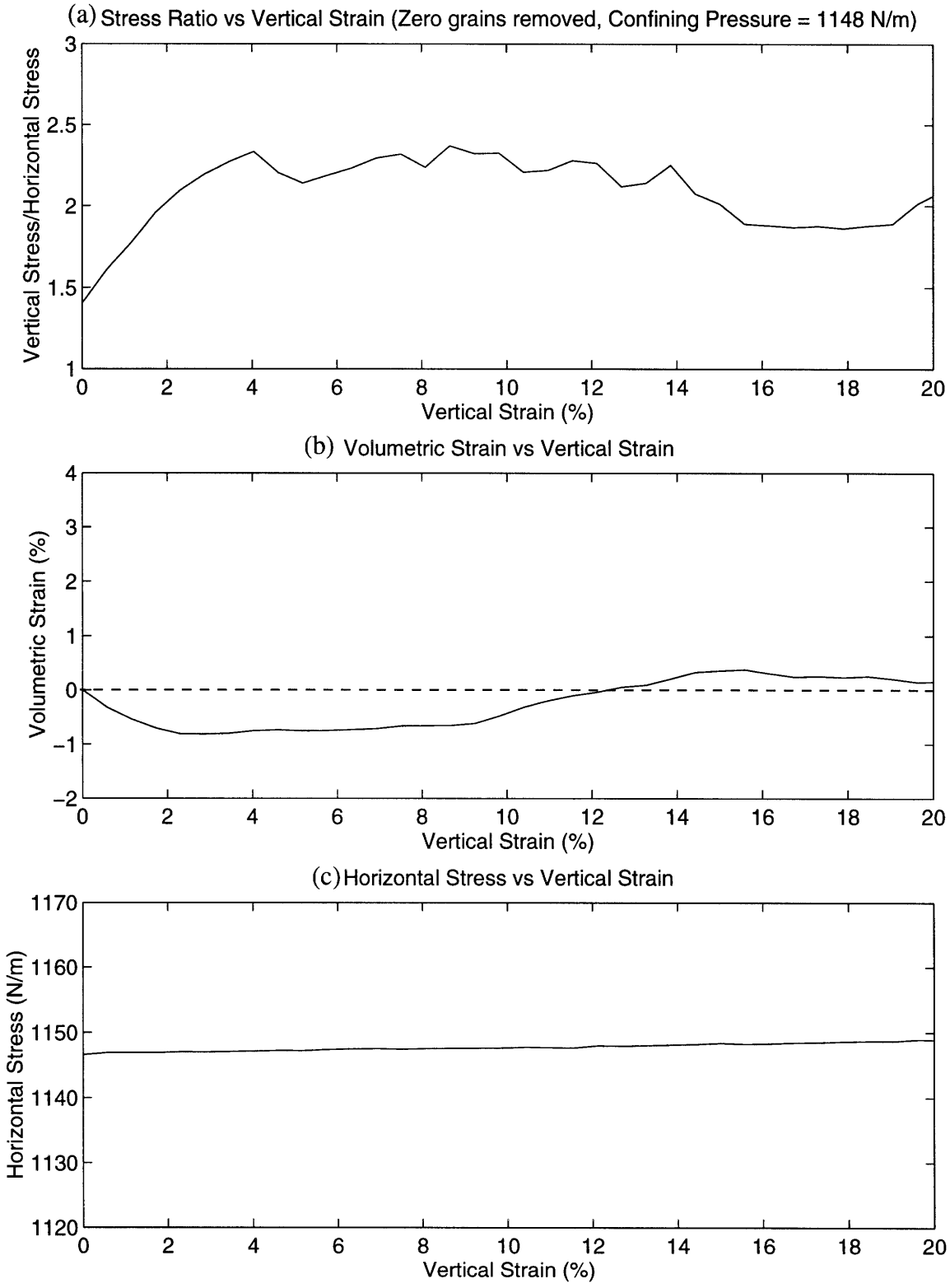

Figure 6.4: Triaxial Results - Zero Particles Removed, Confining Pressure = 1148 N/m

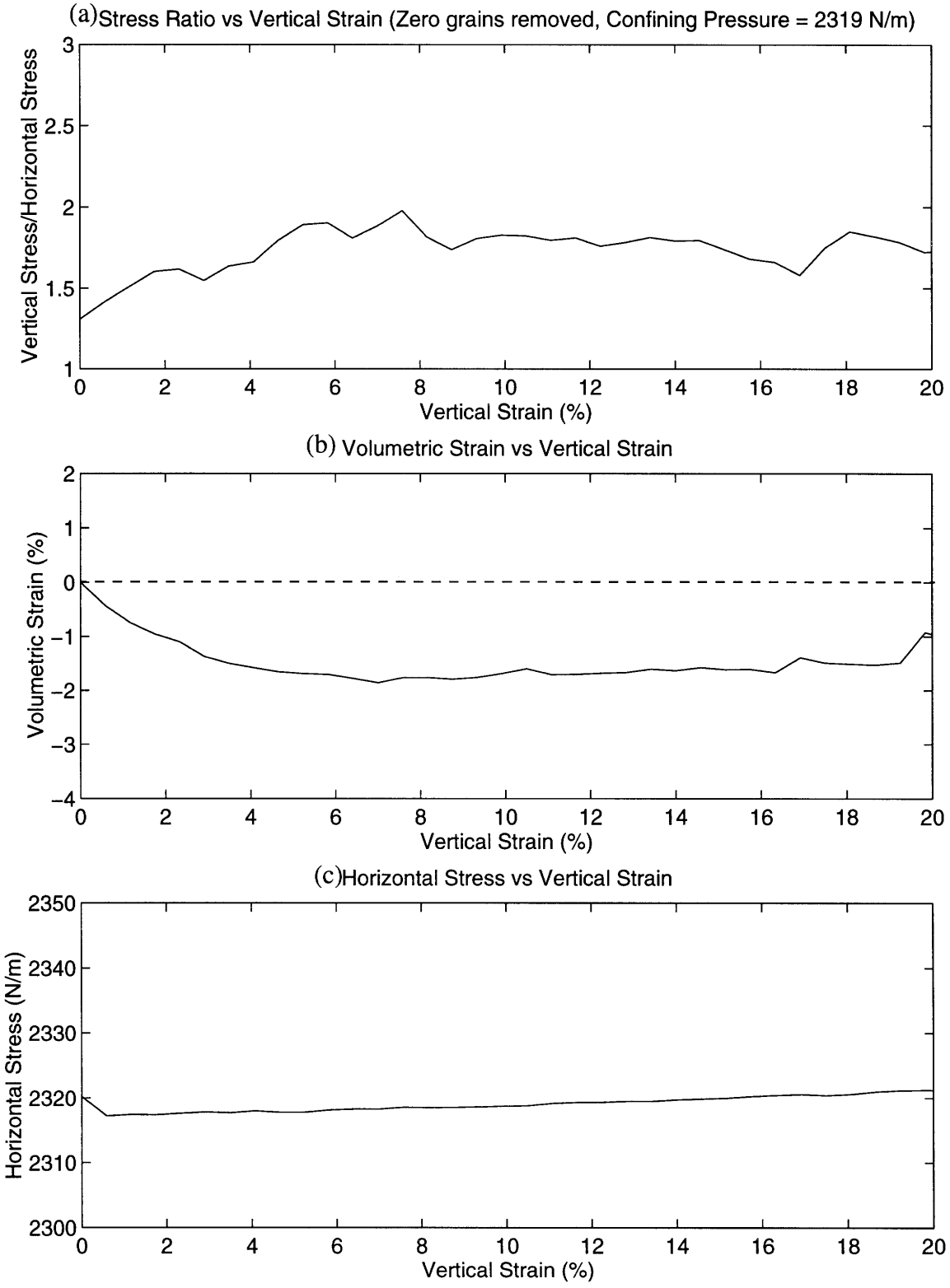

Figure 6.5: Triaxial Results - Zero Particles Removed, Confining Pressure = 2319 N/m

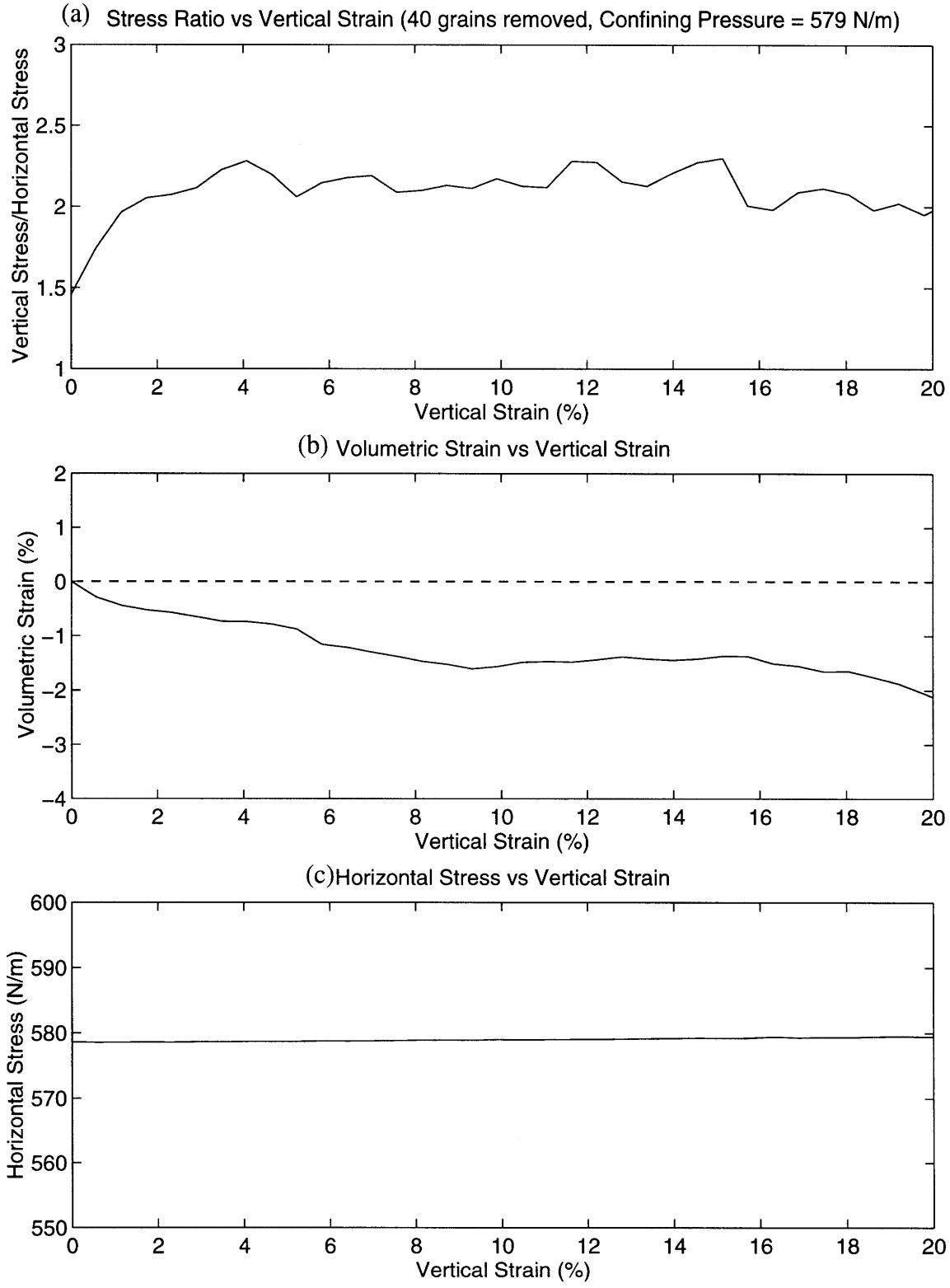

Figure 6.6: Triaxial Results - Forty Particles Removed, Confining Pressure = 579 N/m

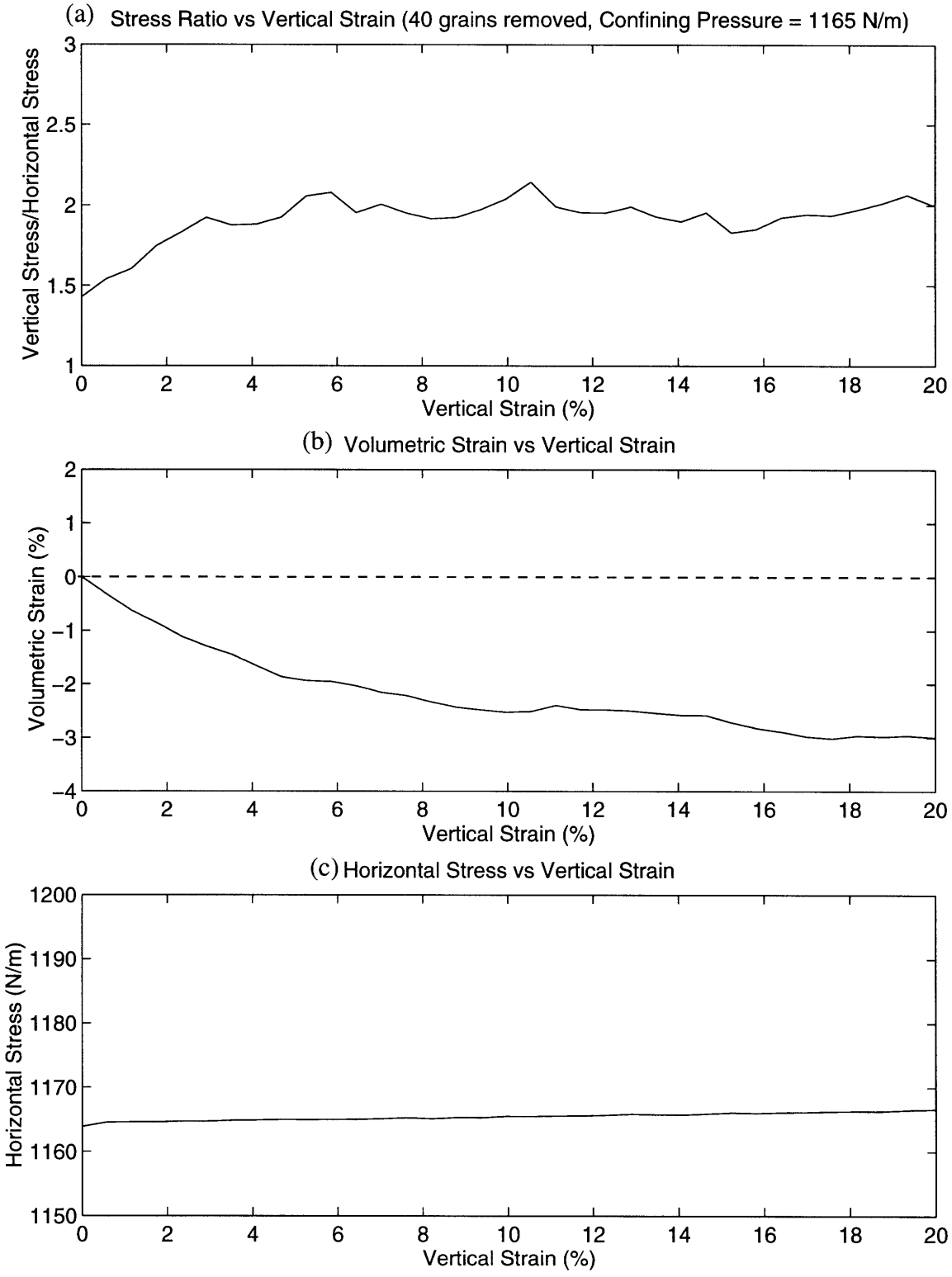

Figure 6.7: Triaxial Results - Forty Particles Removed, Confining Pressure = 1165 N/m

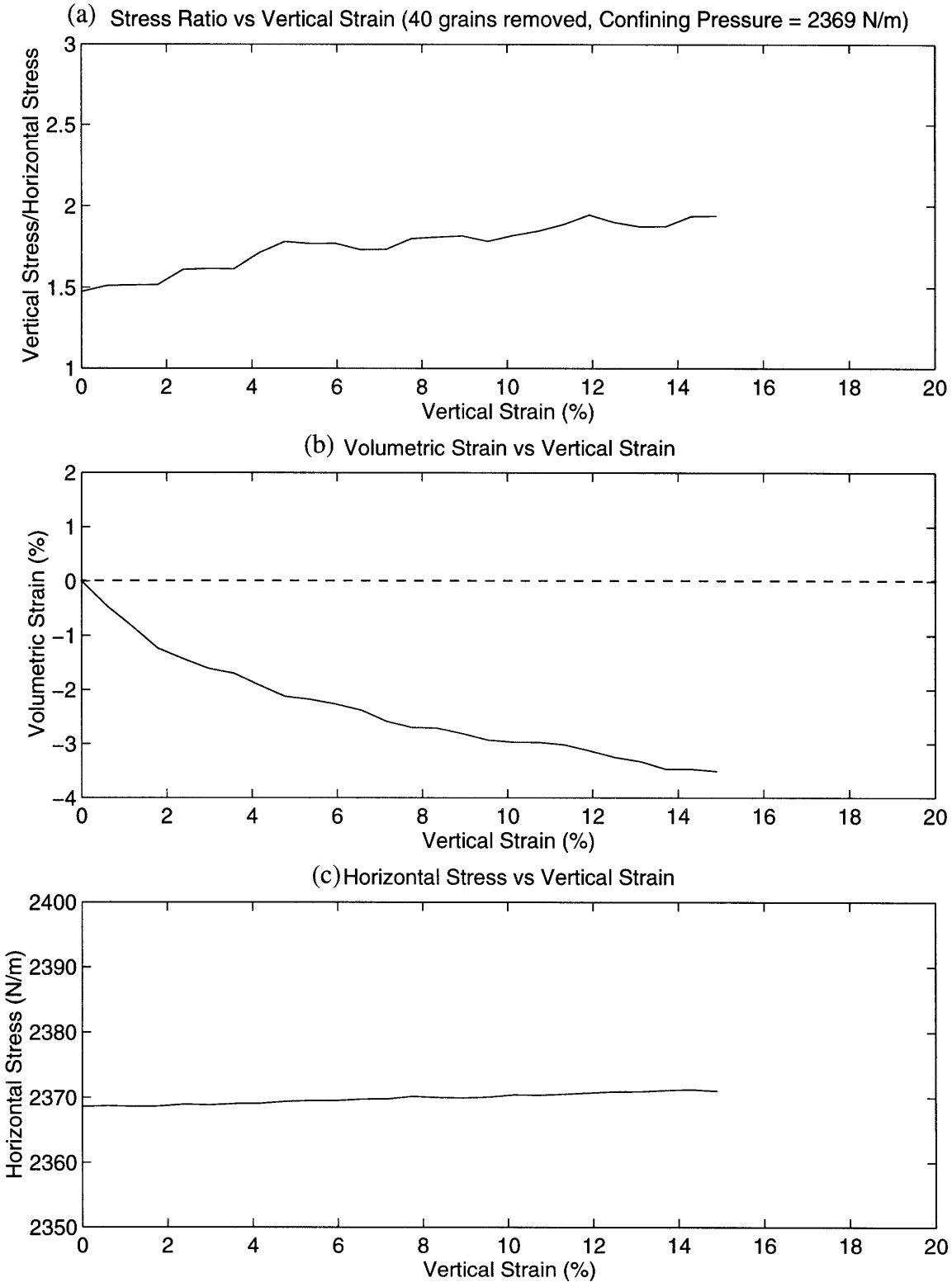

Figure 6.8: Triaxial Results - Forty Particles Removed, Confining Pressure = 2369 N/m

6.4 Effect of Initial Density

The results from the simulations showed that the initial density of the sample has a large influence on the stress-strain behavior of the samples. Plots of the stress ratio versus vertical strain (graph (a)) and volumetric strain versus the vertical strain (graph (b)) are shown in Figures 6.9 to 6.11 These graphs compare the two different densities at each of the three confining stresses. Data for this discussion also come from Tables 6.2 to 6.6. In general, increasing the confining pressure reduced the difference in behavior between samples with different densities.

At all three stresses, the Young's modulus of the denser sample (zero particles removed) was higher than that of the looser sample. This is similar to the one-dimensional compression experiments in Chapter Five where the ratio of stress to strain was higher for denser samples. The greater number of voids in the looser sample provides less resistance to particle rearrangement resulting in a lower stiffness. Since the confining stress is the same for both curves on each plot, all trends that apply to normalized stress also apply to absolute stress.

The next noticeable difference is that the peak stress is higher for the denser samples. This results in a higher friction angle for the denser samples. The peak occurs at a lower strain for the denser samples. These trends agree with extensive experimental data on cohesionless soils.

After failure, only the dense samples underwent strain softening and experienced dilation. After failure, the vertical stress on the looser samples stayed almost constant with increasing vertical strain. The loose samples did not dilate, but the rate of contraction decreased with increasing vertical strain. The dense samples initially contract, but the rate of contraction is less than the loose samples. By the time the failure stress has been

reached, the dense samples have begun to dilate. This rate of dilation reaches a maximum though and approaches zero as the strain increases.

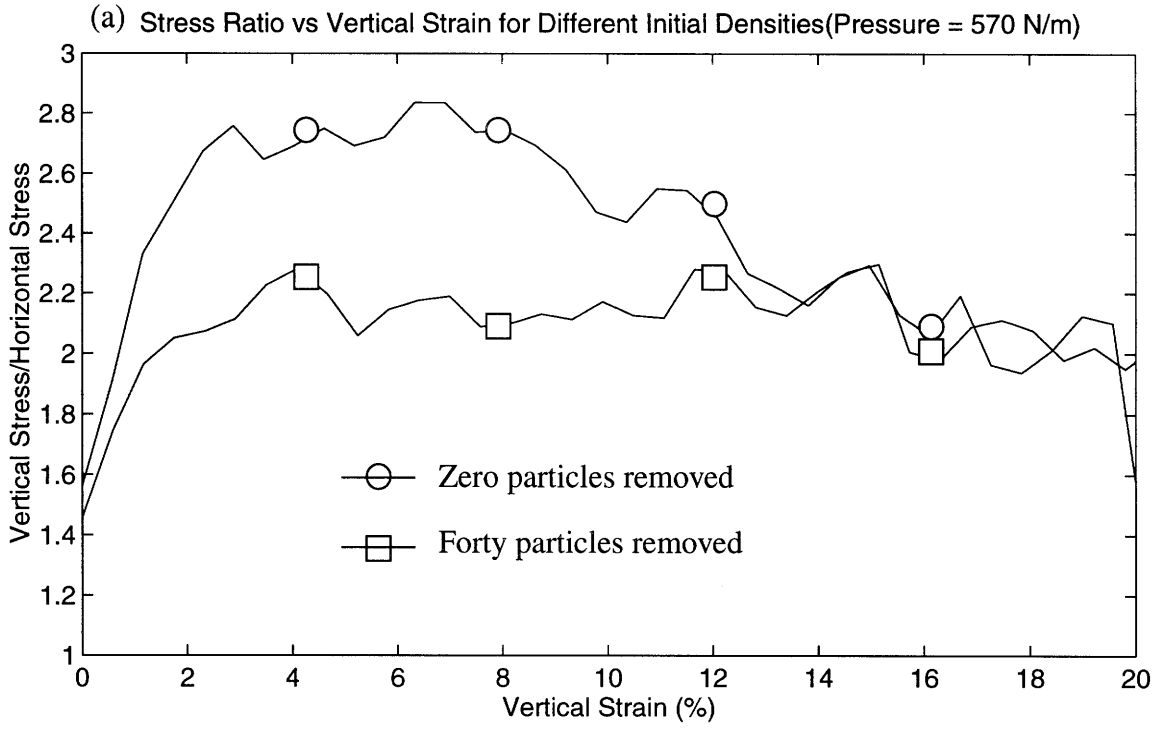

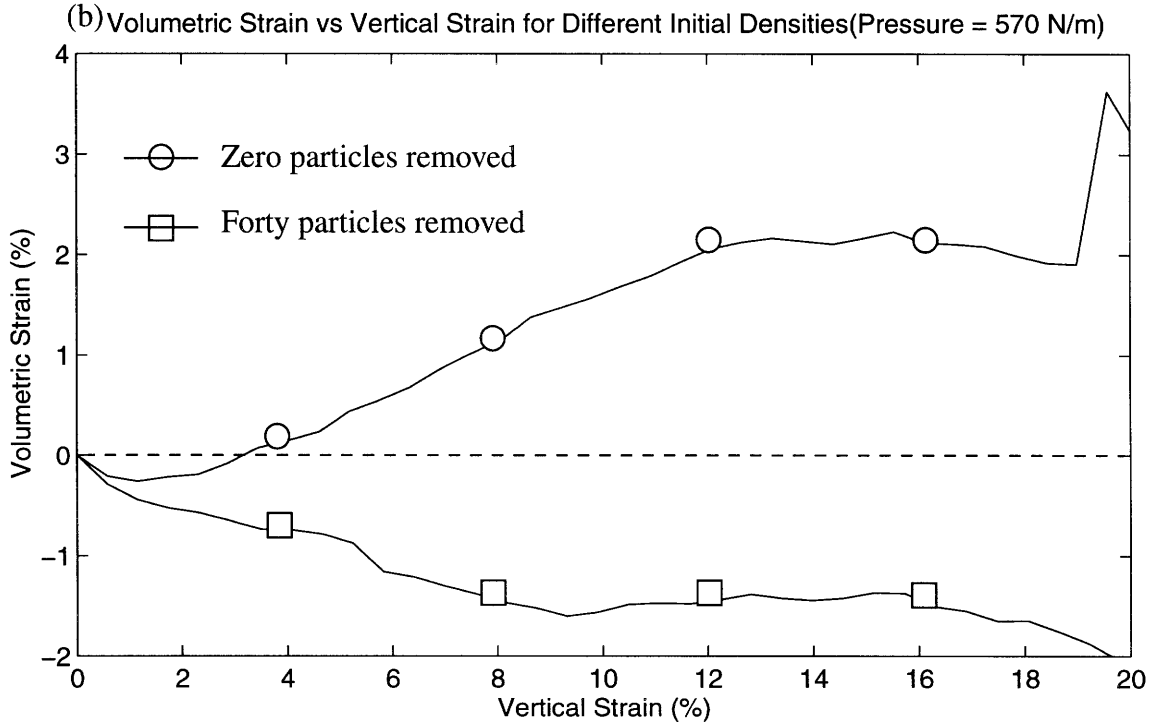

Figure 6.9: Triaxial Results for Different Initial Densities (Confining Stress = 570 N/m

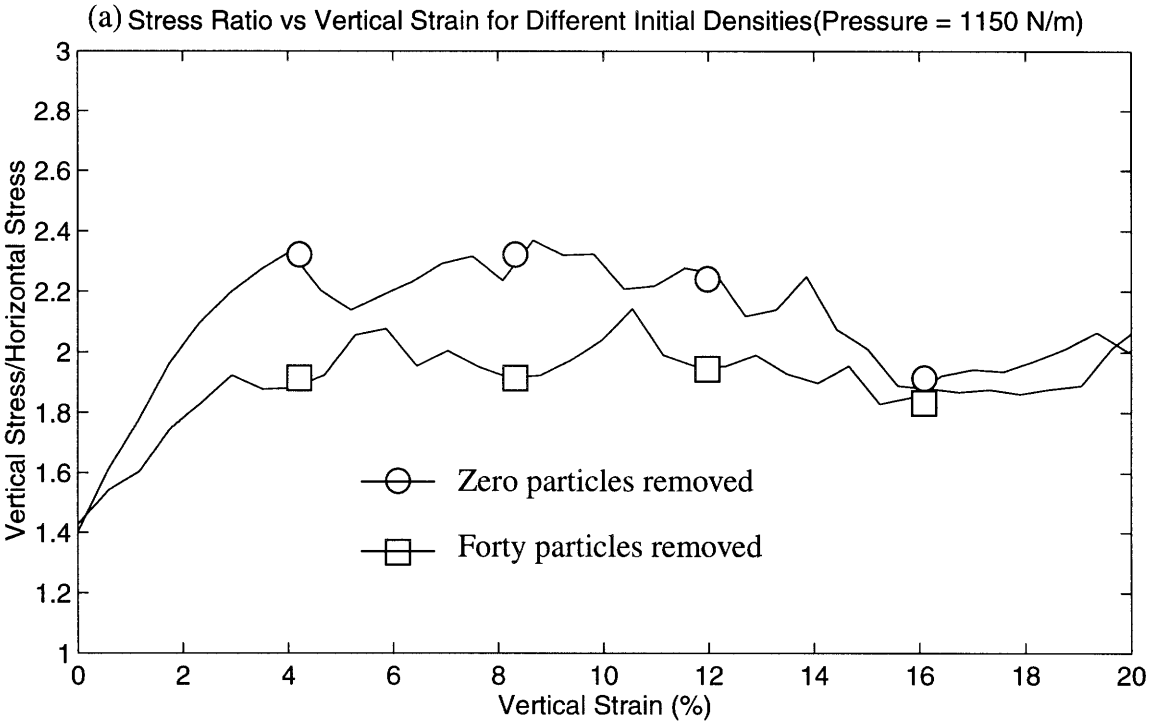

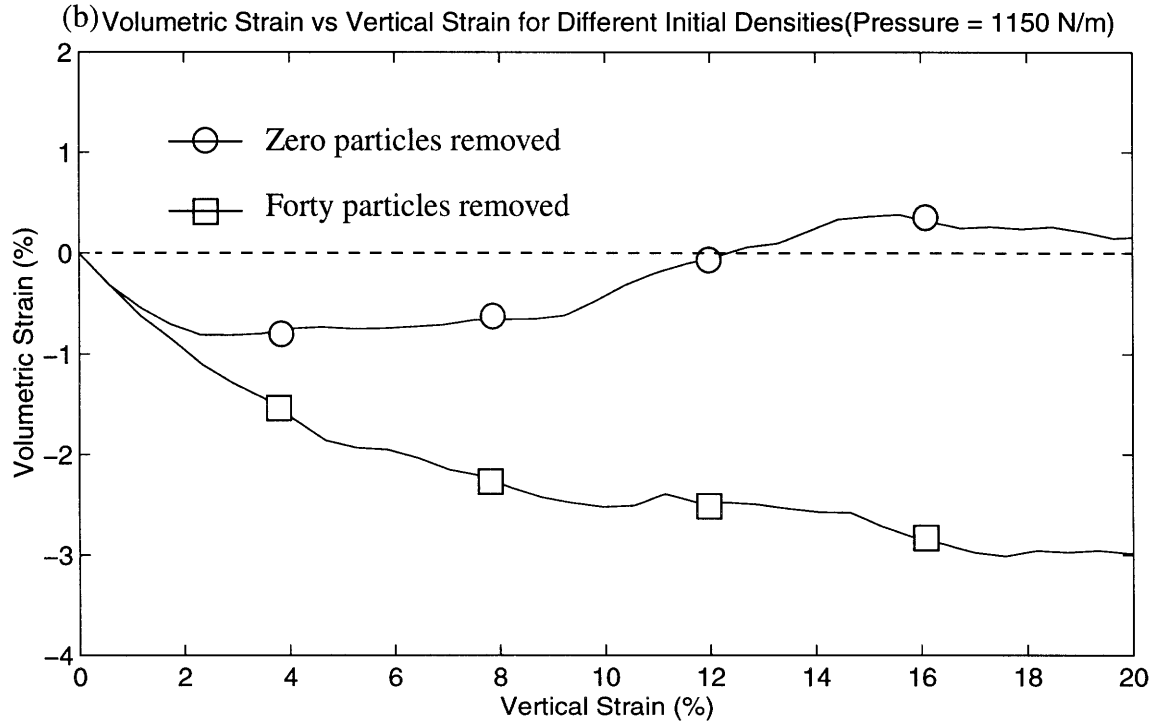

Figure 6.10: Triaxial Results for Different Initial Densities (Confining Stress = 1150 N/m)

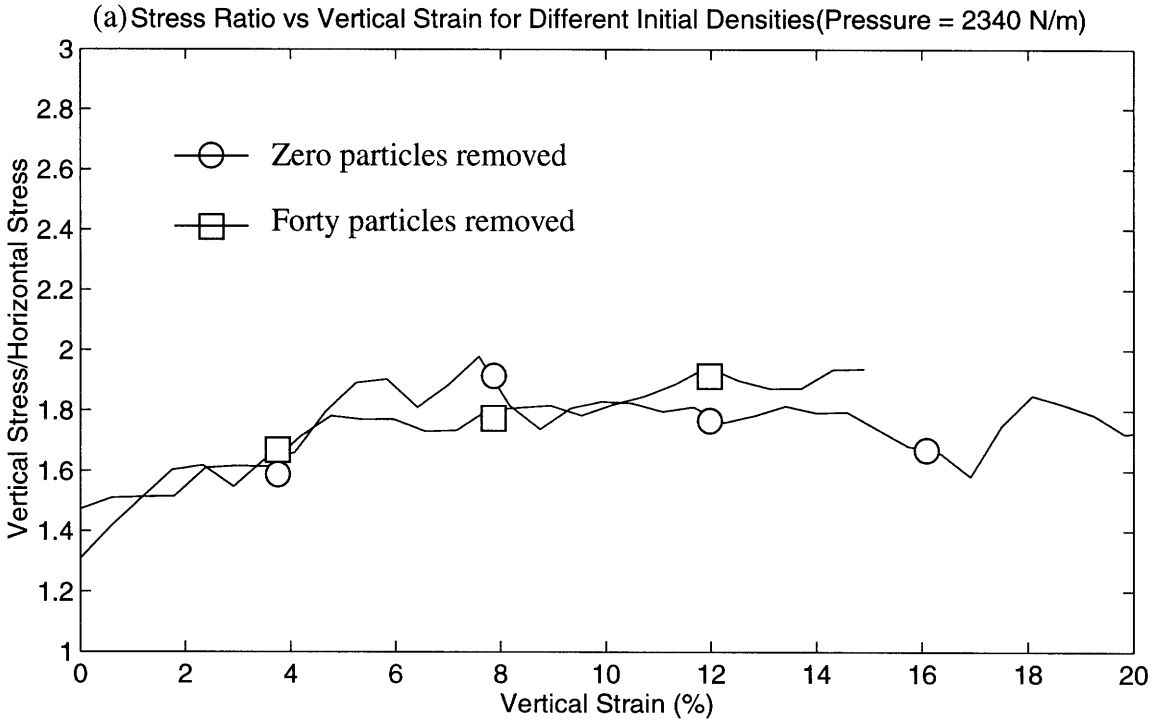

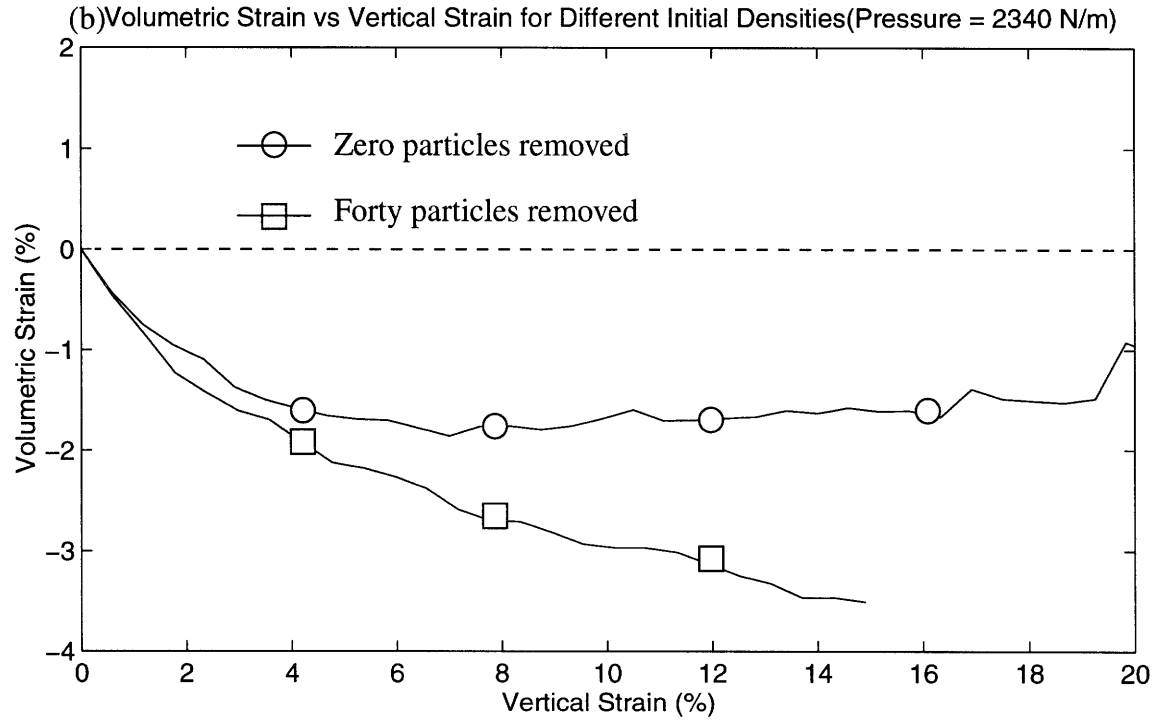

Figure 6.11: Triaxial Results for Different Initial Densities (Confining Stress = 2340 N/m)

6.5 Effect of Confining Stress

The results from the simulations clearly show that the confining pressure also affected the stress-strain behavior of the samples. Plots of the stress ratio versus vertical strain (graph (a)) and volumetric strain versus vertical strain (graph (b)) for each of the three confining stresses are shown in Figures 6.12 (zero particles removed) and 6.13 (forty particles removed). In general, the denser samples show more effects of pressure variation.

For the denser sample, the absolute Young's modulus increased slightly with increasing confining stress. However, the normalized Young's modulus decreased significantly with increasing confining stress. This was not the case for the looser sample, but the smaller peak stresses made the measurement of the Young's modulus from the graphs less reliable for these samples.

The samples with lower confining stress had higher normalized peak stresses. The absolute values were higher with higher confining stress, but the normalized stress determines the friction angle. For this reason, samples with lower confining stresses had higher friction angles. As described in Section 2.6, higher confining stresses inhibit interlocking of particles, thus resulting in lower friction angles.

As described in the Section 6.4, only the dense samples displayed strain softening and dilation. The rate of strain softening was higher for lower confining stresses. These samples also have higher maximum rates of dilation and greater total dilation. For the low density samples, higher confining stresses resulted in greater rates of contraction as well as greater total contraction.

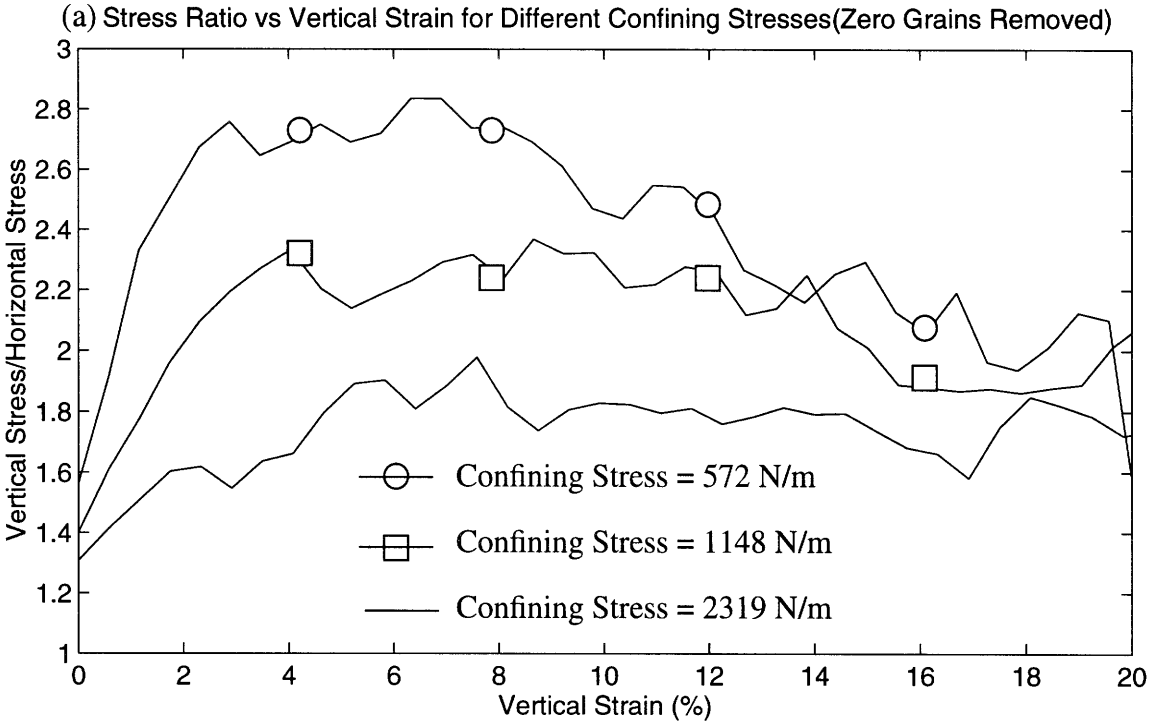

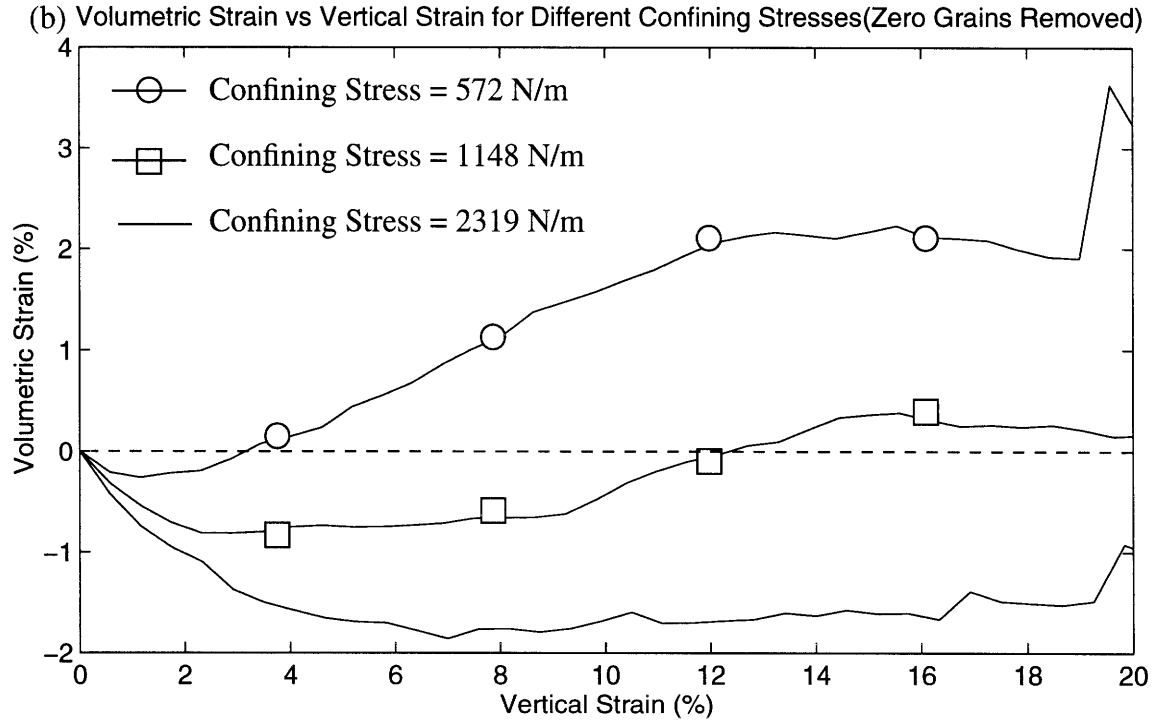

Figure 6.12: Triaxial Results for Different Confining Stresses with No Particles Removed

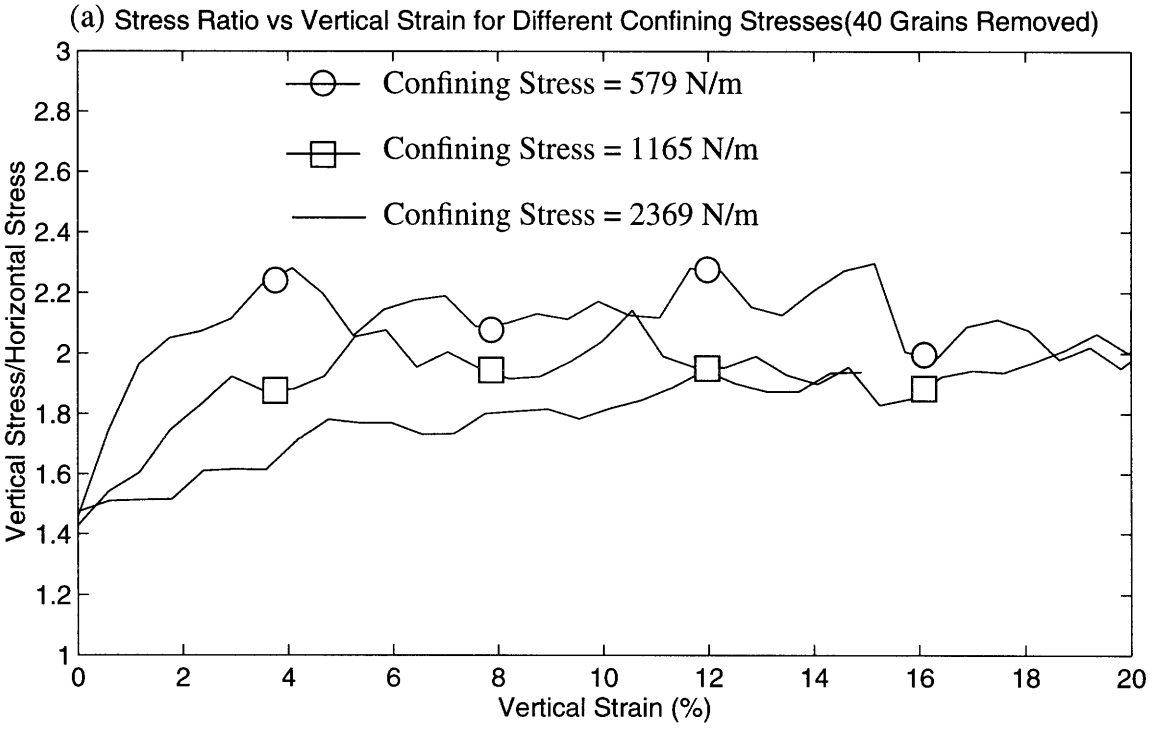

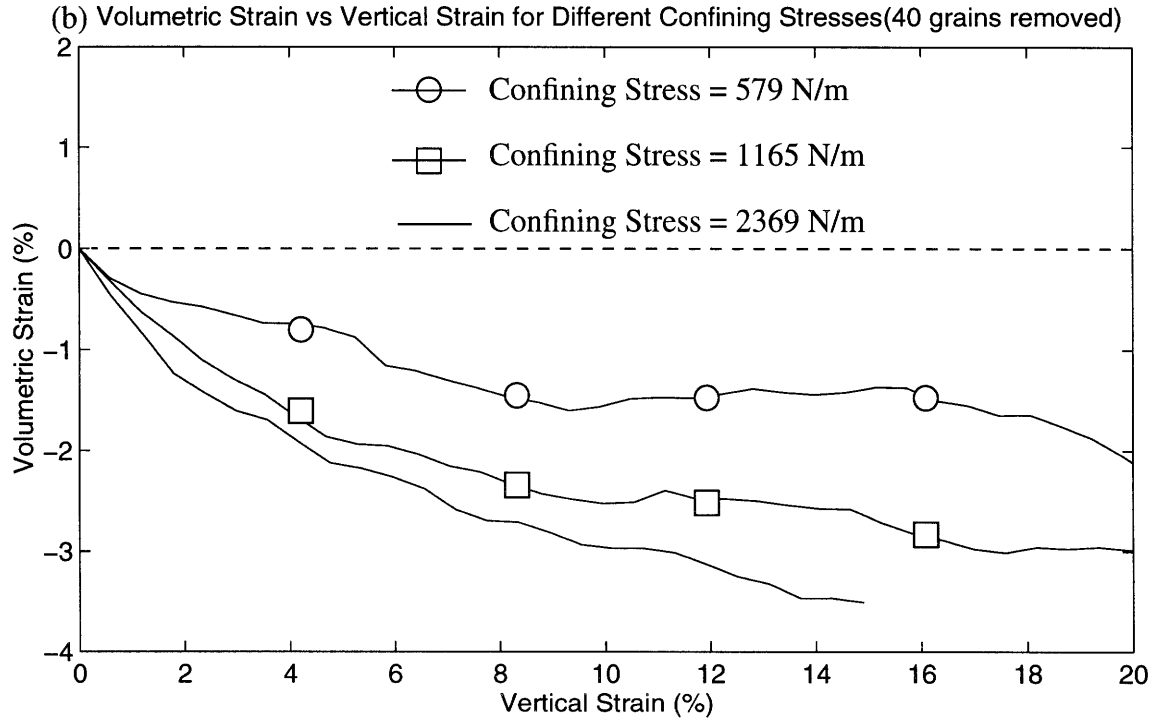

Figure 6.13: Triaxial Results for Different Confining Pressures with 40 Particles Removed

Chapter 7

Summary, Conclusions, and Recommendations

7.1 Summary of Experimental Program and Results

This thesis modeled a number of physical experiments on granular soils using the Discrete Element Method and the MIMES program developed by Williams and Rege (1996). Simulations of multiple sieve pluviation, a "sugar substitution" method to further reduce density, one-dimensional compression tests, and drained triaxial compression tests were reasonably successful in modeling the behavior observed from physical tests on granular soils. These two-dimensional simulations used 800 elliptical shaped disks.

The multiple sieve pluviation (MSP) and "sugar substitution" simulations were performed to control the density of samples. The MSP experiments showed that interparticle friction and the width of the opening on the hopper used to deposit the particles had the greatest influence on the final density of pluviated samples. Higher coefficients of friction created greater shear forces between particles and created looser samples. Decreasing the width of the hopper opening decreased interparticle interference during deposition, resulting in denser samples. Drop height and presence of sieves did not have as significant effects. The simulations displayed the expected trends in controlling density, but the overall range of densities from these experiments was not very large. The "sugar substitution" experiments enabled the creation of samples with much lower densities. Up to eighty particles were removed to simulate physical experiments wherein water dissolves sugar in a sugar-sand mixture. However, there was a lower bound on the number of voids that could be created and still maintain a stable particle packing configuration.

The one-dimensional compression simulations correctly modeled the behavior of the physical tests and showed the effect of density on the process. As samples were com-

pressed, they became increasingly stiffer. The simulations were able to model the compression up to a limiting density after which the system became unstable. Looser samples showed more particle rearrangement during compression. For this reason, samples with higher initial density had higher stiffness and a reached the limiting density at smaller vertical strains.

The drained triaxial compression simulations also had success in modeling physical experiments and showed the effects of both initial density and confining pressure. In general, increasing density and decreasing confining pressure had the same effects on stress-strain behavior. Both resulted in increased normalized Young's modulus, increased normalized failure stress, and greater dilation (or reduced contraction in samples that did not dilate).

Values for the friction angle of the soil were inferred from the one-dimensional compression experiments and measured in the drained triaxial compression tests. The values from both sets of simulations were lower than normally found in three-dimensional soils. The friction angle (calculated from $K_0 = 1 - \sin \phi$) in the one-dimensional compression tests was lower than any of the triaxial values. In the one-dimensional compression tests, the density of the sample did not affect K_0 and hence the inferred friction angle. The triaxial experiments showed that denser samples had higher friction angles, especially at low confining stresses. Increasing confining stress decreased the friction angle.

7.2 Contributions of this Work

A major limitation of Discrete Element simulations of granular materials has been an inability to systematically control the packing density in a realistic manner when preparing samples. The simulations of multiple sieve pluviation confirmed that changing certain experimental parameters generates samples of different densities in a reasonably predict-

able manner. However, the range of parameters used in this thesis did not generate substantial changes of sample densities. It may be possible to increase the range of densities by using a greater range of parameters.

The particle removal process used to simulate sugar substitution proved to be a reliable means of reducing sample density. Since the samples held their shape pretty well after particles were removed, it was possible to remove up to ten percent of the particles until a specific density was reached. There was a minimum density that could be generated with this method, but this might also be reduced with different parameters.

One concern about the particle removal process was whether the soil fabric was representative of a natural deposited state. However, the results from varying density in the one-dimensional compression and drained triaxial compression simulations were consistent with results from physical experiments. This indicates that samples created using this method are representative of actual granular soils with varying densities. Although this method has not been used very much in practice, these results suggest that it is a valid means of creating samples of low density.

The success of the one-dimensional and triaxial compression simulations confirms the ability of the MIMES discrete element program to model the effects of density and confining stress on the behavior of granular materials.

7.3 Future Directions for Research

The experiments in this thesis successfully simulated the physical experiments being modeled and identified the effects of different experimental parameters, but it was not a comprehensive testing program. To further confirm and extend the trends observed here, a greater range of experimental parameters should be used. In the multiple sieve pluviation experiments, a greater range of hopper openings, drop heights, and coefficients of inter-

particle friction might help generate a wider range of densities. Other factors held constant in the experiments in this thesis, such as the distance from the diffuser sieves to the mold and the configuration of the sieves, also could be varied. A greater range of coefficients of friction also could have an effect on the sugar substitution process. All of the simulations could also be run using different particle shapes and sizes and the triaxial tests could also use more confining stresses.

The research could be extended to study the anisotropy of granular soils. The drained triaxial tests could be loaded in the horizontal direction rather than the vertical direction. Undrained shear behavior also can be modeled by varying the vertical and horizontal stresses to obtain no change in the volume of the sample.

Another logical extension of the work presented here would be to look more closely at the behavior of the simulations at the level of individual particles, which is one of the real benefits of the Discrete Element Method. One potential application would be to quantify the effects of interparticle interference in multiple sieve pluviation experiments by measuring the kinetic energy of the individual particles. Rege (1996) has already shown that it is possible to identify the presence of force chains and shear bands by tracking the particles in triaxial compression experiments. These types of measurements might also uncover phenomena at the particle level that are not obvious from the macroscopic data measured at boundaries.

In addition to further experimentation, one of the more important tasks missing from research in DEM simulations of soils testing is to relate actual physical testing data to numbers obtained from simulations. This is particularly difficult with two-dimensional models simulating three-dimensional processes. As described in Section 2.3, there has been significant theoretical research into the packing of two-dimensional particles, but there have been almost no attempts to relate a two-dimensional density to a corresponding

three-dimensional density of particles with similar shapes and dimensions. A greater understanding of the correlation of these densities and the out of plane interaction of particles will be necessary to relate two-dimensional simulations with three-dimensional data. Another option is to continue the development of three-dimensional Discrete Element programs to the point that they can handle a representative sample of particles to model a given application. This would again require significant computing resources, but further improvements in computers should increase the viability of this option.

The field of Discrete Element modeling seems capable of simulating almost any physical process if enough effort is put into including pertinent physical information in a model. To truly reap the benefits of the development of programs, simulations should be run in a wider area of applications. Results from this work will provide a deeper understanding of the physical behavior of granular materials.

Chapter 8

References

[1] Bathe, K.J. *Finite Element Procedures.* Englewood Cliffs, NJ: Prentice-Hall, 1996.

[2] Bojtar, I., and Bagi, K.. "Numerical Evaluation of Internal Variables of Granular Materials." *Micromechanics of Granular Materials.* Shen, H.H., et al, eds. Amsterdam: Elsevier Scientific Publishers. 1992. 331-342.

[3] Christoffersen, J., Mehrabadi, M.M., and Nemat-Nasser, S. "A Micromechanical Description of Granular Material Behavior." *Journal of Applied Mechanics.* Vol. 48, No. 2, June, 1981, 339-344.

[4] Cumberland, D.J. and Crawford, R.J. *Handbook of Powder Technology: The Packing of Particles.* Vol. 6. Williams, J.C. and Allen, T., eds. Amsterdam: Elsevier Science Publishers, 1987.

[5] Cundall, P.A. and Strack, O.D.L. "A Distinct Element Model for Granular Assemblies." *Geotechnique.* Vol. 29, No. 1, March, 1979, 47-65.

[6] Dobry, R. and Ng, T.-T. "Discrete Modelling of Stress-Strain Behaviour of Granular Media at Small and Large Strains." *Engineering Computations.* Vol. 9, No. 2, April, 1992, 129-143.

[7] Gourves, R. "The Analogical Bidimensional Model of Schneebeli. Applications to the Study of Micromechanics of Granular Media." *Advances in Micromechanics of Granular Materials.* Shen, H.H., et al, eds. Amsterdam: Elsevier Scientific Publishers. 1992. 353-362.

[8] Issa, J. A. and Nelson, R. B. "Numerical Analysis of Micromechanical Behaviour of Granular Materials." *Engineering Computations.* Vol. 9, No. 2, April, 1992, 211-223.

[9] Klosek, J. T. *The Integration of Fluid Dynamics with a Discrete-Element Modelling System: Algorithms, Implementation, and Applications.* Master's Thesis, Department of Civil and Environmental Engineering, Massachusetts Institute of Technology, Cambridge, Massachusetts, February 1997.

[10] Ladd, C.C. Personal Communication,1997.

[11] Lambe, T.W. and Whitman, R.V. *Soil Mechanics.* New York: John Wiley and Sons, 1969.

[12] Lee, K.L. and Seed, H.B. "Drained Strength Characteristics of Sands." *Journal of the Soil Mechanics and Foundations Division.* Vol. 93, No. SM6, 1967, 117-141.

[13] Lee, X. and Dass, W. C. "An Experimental Study of Granular Packing Structure Changes Under Load." *Powders and Grains 93.* Thornton, C., ed. Rotterdam: A.A. Balkema. 1993. 17-22.

[14] Lin, X. and Ng, T.-T. "A Three-dimensional Element Model Using Arrays of Ellipsoids." *Geotechnique.* Vol. 47, No. 2, June, 1997, 319-329.

[15] Lo Presti, D. C. F., Pedroni, S., and Crippa, V. "Maximum Dry Density of Cohesionless Soils by Pluviation and by ASTM D4253-83: A Comparative Study." *Geotechnical Testing Journal.* Vol. 15, No. 2, June, 1992, 180-189.

[16] Miura, S. and Toki, S. "A Sample Preparation Method and Its Effect on Static and Cyclic Deformation-Strength Properties of Sand." *Soils and Foundations.* Vol. 22, No. 1, March, 1982, 61-77.

[17] O'Connor, R. *A Distributed Discrete Element Modeling Environment - Algorithms, Implementation, and Applications.* Doctoral Thesis, Department of Civil and Environmental Engineering, Massachusetts Institute of Technology, Cambridge, Massachusetts, January 1996.

[18] Rad, N.S. and Tumay, M.T. "Factors Affecting Sand Specimen Preparation by Raining." *Geotechnical Testing Journal.* Vol. 10, No. 1, March, 1987, 31-37.

[19] Rege, N. V. *Computational Modeling of Granular Materials.* Doctoral Thesis, Department of Civil and Environmental Engineering, Massachusetts Institute of Technology, Cambridge, Massachusetts, February 1996.

[20] Rothenburg, L. and Bathurst, R.J. "Effects of Particle Shape on Micromechanical Behavior of Granular Materials." *Advances in Micromechanics of Granular Materials.* Shen, H.H., et al, eds. Amsterdam: Elsevier Scientific Publishers. 1992. 343-352.

[21] Scott, G.D. "Packing of Spheres." *Nature.* Vol. 188, No. 4754, December 10, 1960, 908-909.

[22] Ting, J. M., Corkum, B. T., Kauffman, C. R., and Greco, C. "Discrete Numerical Model for Soil Mechanics." *Journal of Geotechnical Engineering.* Vol. 115, No. 3, March, 1989, 379-398.

[23] Thornton, C. "Applications of DEM to Process Engineering Problems." *Engineering Computations.* Vol. 9, No. 2, April, 1992, 289-297.

[24] Williams, J. R., O'Connor, R., Preece, D., and Klosek, J. "A Coupled Particle-Fluid Transport Model for Near Wellbore Stability." *Mechanics of Deformation and Flow of Particulate Materials.* Chang, C. S., et al, eds. New York: American Society of Civil Engineers. 1997. 134-148.

[25] Williams, J. R. and Rege, N. "Granular Vortices and Shear Band Formation." *Mechanics of Deformation and Flow of Particulate Materials.* Chang, C. S., et al, eds. New York: American Society of Civil Engineers. 1997. 62-76.